Journal of Volcanology and Geothermal Research 301 (2015) 66–80

Contents lists available at ScienceDirect

Journal of Volcanology and Geothermal Research

journal homepage: www.elsevier.com/locate/jvolgeores

Constraints on the timing of Quaternary volcanism and duration of magma residence at Ciomadul volcano, east–central Europe, from combined U–Th/He and U–Th zircon geochronology

S. Harangi [a,b,*], R. Lukács [a,c], A.K. Schmitt [d], I. Dunkl [e], K. Molnár [b], B. Kiss [a,c], I. Seghedi [f], Á. Novothny [g], M. Molnár [h]

[a] MTA-ELTE Volcanology Research Group, H-1117 Budapest, Pázmány sétány 1/C, Budapest, Hungary
[b] Department of Petrology and Geochemistry, Eötvös University, Budapest, Hungary
[c] Vulcano Research Group, Department of Mineralogy, Geochemistry and Petrology, University of Szeged, Szeged, Hungary
[d] UCLA Department of Earth, Planetary and Space Sciences, Los Angeles, USA
[e] University of Göttingen, Geoscience Center, Sedimentology and Environmental Geology, Göttingen, Germany
[f] Institute of Geodynamics, Romanian Academy, Bucharest, Romania
[g] Department of Physical Geography, Eötvös University, Budapest, Hungary
[h] Hertelendi Laboratory of Environmental Studies, Institute for Nuclear Research of the Hungarian Academy of Sciences, Debrecen, Hungary

ARTICLE INFO

Article history:
Received 21 January 2015
Accepted 7 May 2015
Available online 19 May 2015

Keywords:
U–Th disequilibrium age dating
(U–Th)/He age dating
Infrared stimulated luminescence dating
Zircon
Magma chamber
Volcanic eruption chronology

ABSTRACT

High-spatial resolution zircon geochronology was applied to constrain the timescales of volcanic eruptions of the youngest, mostly explosive volcanic phase of Ciomadul volcano (Carpathian–Pannonian region, Romania). Combined U–Th and (U–Th)/He zircon dating demonstrates that intermittent volcanic eruptions occurred in a time range of 56–32 ka. The reliability of the eruption dates is supported by concordant ages obtained from different dating techniques, such as zircon geochronology, radiocarbon analysis, and infrared stimulated luminescence dating for the same deposits. The new geochronological data suggest that volcanism at Ciomadul is much younger (<ca. 200 ka) than previously thought (up to 600 ka). A dominantly explosive volcanic phase occurred after an apparent lull in volcanism that lasted for several 10's of ka, after a period of lava dome extrusion that defines the onset of the known volcanism at Ciomadul. At least four major eruptive episodes can be distinguished within the 56–32 ka period. Among them, relatively large (sub-plinian to plinian) explosive eruptions produced distal tephra covering extended areas mostly southeast from the volcano. The 38.9 ka tephra overlaps the age of the Campanian Ignimbrite eruption and has an overlapping dispersion axis towards the Black Sea region. The wide range of U–Th model ages of the studied zircons indicates prolonged existence of a low-temperature (<800 °C) silicic crystal mush beneath Ciomadul. The main zircon crystallization period was between ca. 100 and 200 ka, coeval with the older, mostly extrusive lava dome building stage of volcanism. Even the youngest U–Th model ages obtained for the outermost 4 μm rim of individual zircon crystals predate the eruption by several 10's of ka. The zircon age distributions suggest re-heating above zircon saturation temperatures via injection of hot mafic magmas prior to eruption. Intermittent intrusions of fresh magma could play a significant role in keeping the intrusive silicic magmatic reservoir in a partially melted for prolonged period. The previous history of Ciomadul suggests that melt-bearing crystal mush resided beneath the volcano, and was rapidly remobilized after a protracted (several 10's of ka) lull in volcanism to trigger several eruptions in a comparatively short time window. This classifies Ciomadul as a volcano with 'Potentially Active Magma Storage' (PAMS) which we propose to be common among the seemingly inactive volcanoes in volcanic arc regions. The potential for reactivation of these systems should be included into volcanic hazard assessments.

1. Introduction

Evaluation of volcanic hazard is often difficult, particularly in regions where no volcanic events have been documented in historical times or even longer. Continental Europe (excluding Italy and Greece) is such a region, where the most recent volcanic eruptions occurred between ca. 6.5 and 40 ka in western Germany (Eifel), eastern–central France

* Corresponding author at: Department of Petrology and Geochemistry, Eötvös University, Budapest, Hungary. Tel.: +36 1372 2500x8355; fax: +36 1381 2108.
E-mail address: szabolcs.harangi@geology.elte.hu (S. Harangi).

http://dx.doi.org/10.1016/j.jvolgeores.2015.05.002
0377-0273/

(Massif Central), and Garrotxa, northeast Spain (van den Bogaard, 1995; Nowell et al., 2006; Schmincke, 2007; Puiguriguer et al., 2012). However, long recurrence rates of volcanism notwithstanding, the evidence for protracted high-temperature crystallization of zircon for 10's of ka for Laacher See volcano (Eifel; Schmitt, 2006) implies that further volcanic events cannot be unequivocally excluded for these areas. Therefore, more careful studies are necessary to reveal the nature of this kind of volcanism with low magma fluxes and sporadic eruptions.

Here, we present new geochronological results based on U–Th and (U–Th)/He zircon data and infrared stimulated luminescence (IRSL) dating on feldspar, and demonstrate that relatively young, intermittent volcanic eruptions occurred also at Ciomadul volcano (eastern Carpathians, Romania), eastern–central Europe in a time range of 56–32 ka. In contrast to the intra-continental tectonic setting of the above listed European volcanic regions, Ciomadul has a post-collisional setting and is located close to the seismically active Vrancea zone interpreted by some to represent a slab remnant (Szakács and Seghedi, 2013; cf. Fillerup et al., 2010). The new ages also reveal that large explosive eruptions occurred at Ciomadul during the 56–32 ka period which coincides with wide-spread tephra deposition originating from volcanoes in central Italy. We argue that Ciomadul eruptions produced tephras which possibly cover extended areas in central–eastern and south–eastern Europe and thus can provide important yet currently unrecognized marker horizons for tephrochronologic studies. Although no more volcanic eruptions of Ciomadul are known since ca. 32 ka, a seismic tomography model (Popa et al., 2012) as well as combined petrologic and magnetotelluric studies (Harangi et al., 2015) indicate that a melt-bearing magma body could have persisted beneath the volcano to the present day. Petrogenetic models (Kiss et al., 2014) indicate that silicic magma likely resided as a crystalline mush at mid-crustal depth long before the eruptions, and possibly after. Thus, precise dating of the past volcanic activity and the longevity of the magma reservoir is crucial to understand the nature of volcanoes with potentially active magma storage (PAMS; Harangi et al., 2015) such as Ciomadul, and evaluate their volcanic hazards.

2. Geological setting

The Ciomadul volcano is located at the southeastern edge of the Carpathian–Pannonian region (CPR, Fig. 1; Szakács et al., 1993; Szakács and Seghedi, 1995; Karátson et al., 2013; Kiss et al., 2014; Harangi et al., 2015; Szakács et al., 2015) and is composed of about 8–14 km^3 dacitic eruptives (Karátson and Timár, 2005; Szakács et al., 2015). In the CPR, a compositionally wide range of magmas erupted during the last 20 Ma (Szabó et al., 1992; Harangi, 2001; Seghedi et al., 2004, 2005; Harangi and Lenkey, 2007; Lexa et al., 2010; Seghedi and Downes, 2011). During the Quaternary, eruptions occurred mostly along the peripheral areas of the CPR. The youngest volcanoes developed at the southern termination of the Călimani–Gurghiu–Harghita (CGH) andesitic–dacitic volcanic chain (Szakács and Seghedi, 2013). Shoshonitic magmas formed isolated cryptodome bodies at ca. 1.5 Ma (e.g., Mason et al., 1995; Pécskay et al., 1995; Mason et al., 1996) followed by intermittent extrusions of dacitic lava domes since ca. 1 Ma (Pécskay et al., 1992, 1995; Szakács et al., 2015; Fig. 2). The Ciomadul volcano is the youngest manifestation of volcanic activity in the CPR and it forms the Ciomadul Lava dome Complex (CLC) with the 0.5–1.0 Ma "satellite" lava domes (Fig. 2).

The geodynamic setting of the CGH volcanism and particularly the eruptive activity of the southern end-members of that chain, the Harghita and Ciomadul volcanoes, is highly debated. The volcanism along the CGH chain is characterized by gradually southward younging volcanism <11.3 Ma (Peltz et al., 1987; Pécskay et al., 1995) and post-dates the purported subduction during the mid Miocene (Cloetingh et al., 2004). Thus, the CGH volcanic activity is considered post-collisional (Mason et al., 1996; Seghedi and Downes, 2011). There was a sharp compositional change of the erupted magmas within the Harghita Mountains at ca. 3 Ma and since that time more potassic and incompatible element-enriched magmas erupted (Seghedi et al., 1987; Szakács et al., 1993; Mason et al., 1996). The Ciomadul volcano is located about 50 km from the Vrancea zone (Fig. 1B) that exhibits the largest present-day strain concentration in continental Europe (Wenzel et al., 1999; Ismail-Zadeh et al., 2012). Frequent earthquakes with deep hypocentres beneath Vrancea are consistent with a dense and cold

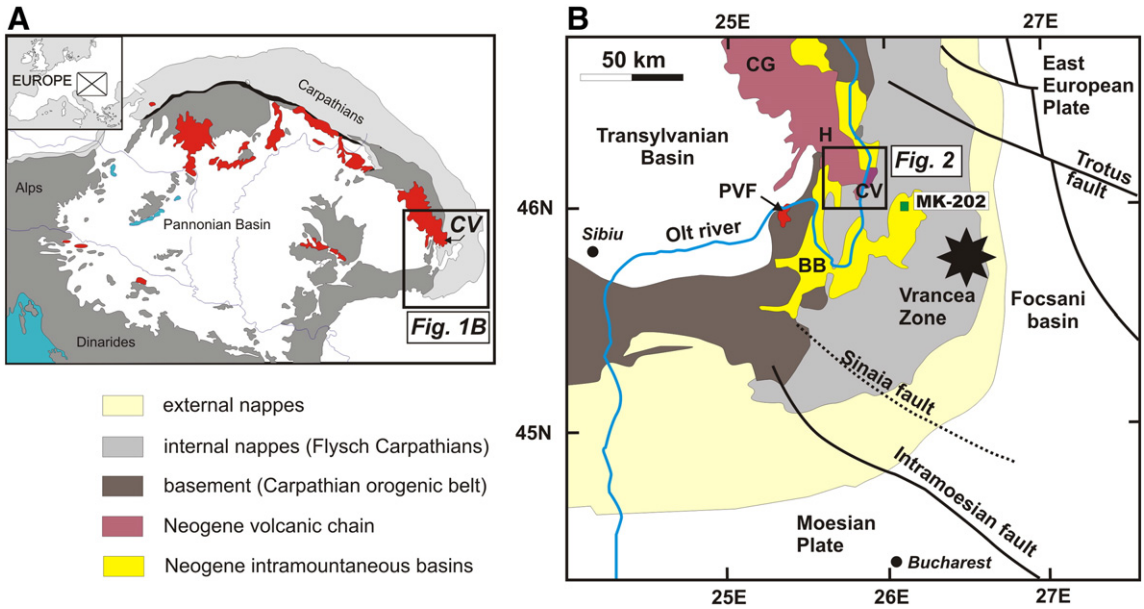

Fig. 1. Location of the Ciomadul volcano (CV) in the Carpathian–Pannonian Region (red colour in Fig. 1A denotes the Miocene to Pliocene andesite–dacite volcanoes). CG = Călimani-Gurghiu volcanic complex, H = Harghita volcanic complex, BB = Brașov basin, PVF = Perșani basalt volcanic field. Geological map was drawn after Cloetingh et al. (2004) and Martin et al. (2006). Location of the distal tephra sample location, MK-202 (46°1′6.10″É-26°7′20.45″K), is also indicated. The Vrancea zone is a seismically active area due to a descending vertical slab in the upper mantle.

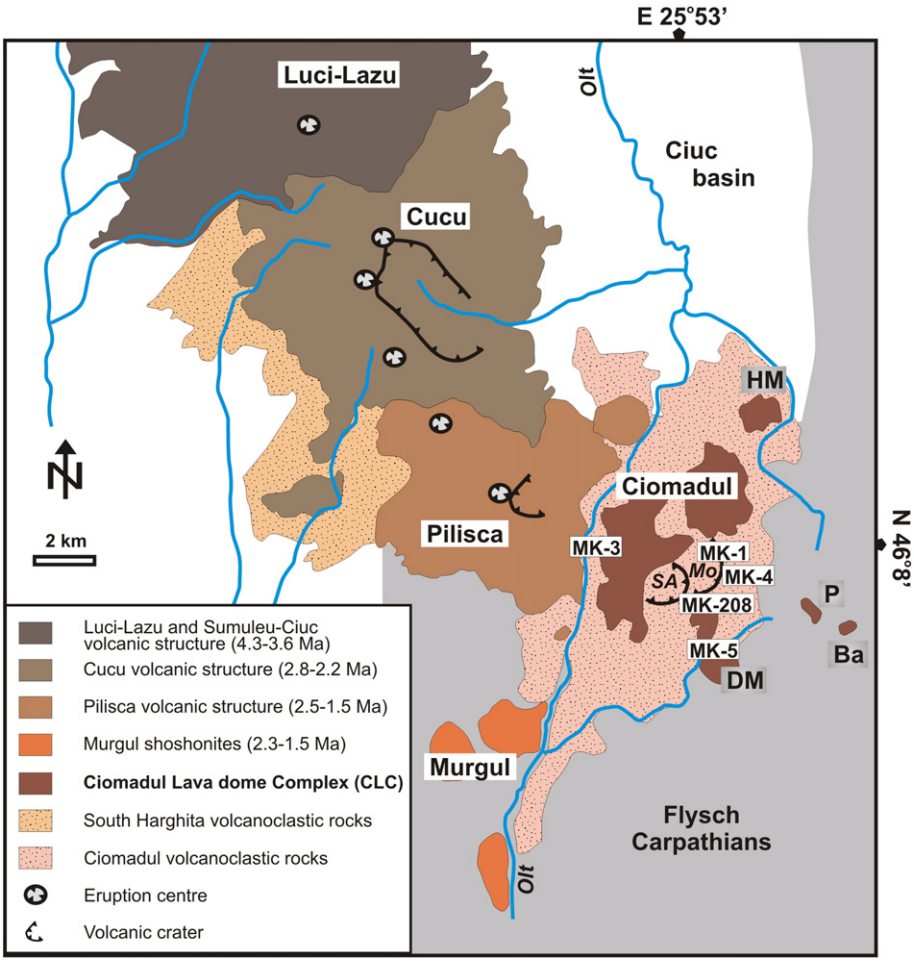

Fig. 2. Simplified geological map of the southern margin of the eastern Carpathians with the location of the Ciomadul volcano (after Seghedi et al., 1987) and the localities of samples. Geographical coordinates are the following: MK-1: 46°08′10.80″N-25°54′34.91″E; MK-3: 46°07′54.89″N-25°5135.09″E; MK-4: 46°07′45.50″N-25°55′54.51″E; MK-5: 46°6′37.42″N-25°54′45.31″E; and MK-208: 46°7′14.74″N-25°54′12.30″E. The South Harghita volcanic field comprises the Luci–Lazu, Cucu and Pilisca volcanic complexes. The Ciomadul Lava dome Complex (CLC) as defined here comprises the Ciomadul volcano and the surrounding lava domes (HM = Haramul Mic; P = Puturosul; Ba = Balvanyos; DM = Dealul Mare).

Fig. 3. The explosion crater of the Ciomadul thought to be formed by a sub-plinian to plinian eruption at 39 ka. The crater is presently filled by the Sf. Ana lake. In the front, there is the Mohos swamp, which fills the older crater of Ciomadul. Photo courtesy of István Fodor.

slab descending near-vertically into the upper mantle (Oncescu et al., 1984; Sperner et al., 2001; Martin et al., 2006; cf. Fillerup et al., 2010) and pose a persistent regional seismic hazard. Volcanic activity of Ciomadul and the nearby Persani basalt volcanic field (Downes et al., 1995; Harangi et al., 2013; PV in Fig. 1B) could be also related to this active tectonic setting, although the link between the vertical slab movement, magma generation, and volcanism is still unclear.

During the first Ciomadul volcanic stage, dacitic magmas extruded and coalesced into a lava dome complex. This was followed by a more explosive volcanic stage, when two deep craters were excavated, the Mohos and the Sf. Ana craters (Fig. 3.; Szakács et al., 1993; Szakács and Seghedi, 1995; Karátson et al., 2013; Szakács et al., 2015). Subplinian and vulcanian explosive eruptions (Szakács et al., 2015) were accompanied by further lava dome extrusions and multiple dome collapses depositing pumiceous block-and-ash flows (Vinkler et al., 2007). These hot pyroclastic flows occasionally charred wood producing charcoal amenable to ^{14}C dating of the eruptions (Moriya et al., 1995, 1996; Vinkler et al., 2007; Harangi et al., 2010). The high-K dacitic magmas of Ciomadul remained fairly homogeneous through time (Szakács and Seghedi, 1986; Vinkler et al., 2007). Plagioclase, amphibole and biotite are the main phenocrysts phases accompanied by apatite, titanite, zircon and the occasional occurrence of quartz, K-feldspar, olivine, clinopyroxene and orthopyroxene. This mineral assemblage indicates mixing of antecrysts from a silicic crystal mush with crystals originating from basaltic recharge and in-situ crystallization in the resulting hybrid magmas (Kiss et al., 2014).

The K–Ar and Ar–Ar data (Pécskay et al., 1992, 1995; Karátson, 2007; Szakács et al., 2015) indicate prolonged volcanism of the Ciomadul volcano since about 600 ka. Preliminary (U–Th)/He and U–Pb zircon ages published in Karátson et al. (2013) suggest that initiation of volcanism could not be older than ca. 250 ka, although these dates were uncorrected for U-series disequilibrium and thus stand as minimum ages for the eruptions. Radiocarbon dating of charcoal fragments embedded in pumiceous pyroclastic deposits implies eruptions as young as 42–32 ka (Moriya et al., 1995, 1996; Vinkler et al., 2007; Harangi et al., 2010). Unfortunately, charcoal fragments are rare and therefore additional constraints on the timing of the youngest volcanic cycle are required.

3. Samples and methods

3.1. Sampling and locations

Identification of the volcanic products from distinct eruptions at Ciomadul is hampered by scarce outcrops due to dense forest vegetation and the homogeneous mineral and bulk rock chemical compositions of the dacite. In this study, we focused primarily on pyroclastic deposits, both in proximal and distal locations (Figs. 1B and 2). These deposits result partly from pyroclastic flows related to explosive collapse of lava domes and from fall-out of crater-forming eruptions. To directly compare pyroclastic flow ages to a potential source dome, we also sampled a remnant of a morphologically pristine lava dome (Kövesponk) at the southern rim of the Sf. Ana crater even though it was considered to be developed during the early stage (290–560 ka) of Ciomadul volcanism based on K/Ar dating by Pécskay et al. (1992) and Szakács et al. (2015). MK-208 zircons were separated from the crystal-rich dacite of this lava dome. Sample MK-5, collected at the southern margin of the Ciomadul volcano (3 km from Bixad, along the road 113 to the lake St. Ana) is of primary interest because this pumiceous pyroclastic flow deposit yielded abundant charcoal fragments used for ^{14}C dating (Vinkler et al., 2007; Harangi et al., 2010). We have previously dated five differently-sized (4–60 cm) charcoal fragments and obtained concordant results averaging 31.5 ± 0.3 ka cal BP (Harangi et al., 2010). These concordant charcoal ages provide a benchmark with which we compare the (U–Th)/He zircon eruption ages determined on crystals separated from large pumice blocks (5–15 cm in size) from the same location. The sample MK-1, too, represents a pyroclastic flow deposit (denoted as bed M3 by Karátson, 2007) which is exposed at the eastern margin of the Mohos crater in the ravine of the rivulet Veres (Fig. 4). Zircons were extracted from a single 20-cm sized pumice block from the middle of a massive (~3 m thick) bed. The pyroclastic flow deposit is overlain by volcanic and lacustrine layers thought to have accumulated within the crater lake (Karátson, 2007; Vinkler et al., 2007). Karátson (2007) conducted Ar–Ar dating on biotites separated from pumice clasts of a pyroclastic fall layer located 1.5 m above the pyroclastic flow deposit and obtained an age of 270 ± 20 ka.

MK-3, MK-4, and MK-202 represent composite pumice samples from pyroclastic fall-out deposits. Sample MK-3 (pumices with 3–5 cm in size) was collected from a pumiceous fall-out layer, which occurs beneath a massive pyroclastic flow deposit at the western margin of the Ciomadul (1.5 km south from Baile Tusnad, at the road E578, in an abandoned quarry; Fig. 7. in Szakács et al., 2015). A 2 cm sized charcoal fragment was previously collected from the pyroclastic flow deposit ~1 m above the pyroclastic fall layer, and dated at 41.1 ± 0.8 ka cal BP (Harangi et al., 2010). The outcrop of sample MK-4 is located east of Mohos crater (close to the road 113A; Fig. 2), where a 2.5 m thick sequence of pyroclastic fall and surge layers with variable thicknesses is exposed. Pumices (3–10 cm in size) were collected from a 1.5 m thick, well sorted pumice fall deposit at the base of this unit. In addition to these proximal pyroclastic products, we collected a composite pumice sample (individual clasts 1–2 cm in size) from a distal fall-out layer, 22 km southeast from the volcano and close to the village of Târgu Secuiesc (Kézdivásárhely; MK-202; Vinkler et al., 2007). This 20–25 cm thick, well-sorted tephra bed occurs in a massive sandy deposit. This tephra was associated with a relatively large explosive eruption which possibly excavated the Sf. Ana crater (Vinkler et al., 2007).

All samples contain the same mineral assemblage, i.e. dominant plagioclase, amphibole and biotite phenocrysts and common accessory minerals such as apatite, titanite, and zircon (Vinkler et al., 2007; Kiss et al., 2014). Sample MK-208 also contains felsic crystal clots comprising plagioclase, amphibole, titanite, and zircon.

3.2. Sample preparation

Approximately 1 kg of rock was collected from each outcrop. Samples were crushed and sieved to <250 μm. A shaking table was used for the <250 μm fraction, and the heaviest fraction was immersed in heavy liquid (sodium polytungstate with a density of 2.90 g/cm^3). Zircon was concentrated by magnetic separation using a Frantz isodynamic separator. Inclusion- and fissure-free intact zircon crystals >70 μm in width were hand-picked from the non-magnetic fraction under a binocular microscope, photographed and packed into platinum (Pt) capsules for He degassing; from the same concentrates ~100 zircon crystals per sample were hand-picked and mounted in an epoxy disk. The studied zircons have a maximum length of 330 μm (mostly in the samples of MK-3 and MK-5) with a minimum length of 240 μm (mostly in the samples of MK-1 and MK-202). The average aspect ratio (length/width) is ~3:1, with the exception of zircon crystals from the MK-208 lava dome samples with an aspect ratio of ~2:1. The cathodoluminescence and back-scattered images of zircons were taken using an AMRAY 1830 type SEM + EDAX PV9800 EDS equipped with a GATAN MiniCL at the Department of Petrology and Geochemistry, Eötvös University.

3.3. (U–Th)/He analysis

(U–Th)/He age determinations were carried out at the University of Göttingen. Zircon crystals were heated inside Pt capsules for 5 min under high vacuum using an infra-red laser. The extracted gas was purified using a SAES Ti-Zr getter at 450 °C. The chemically inert noble gases and a minor amount of other residual gases were then expanded into a Hiden triple-filter quadrupole mass spectrometer equipped with

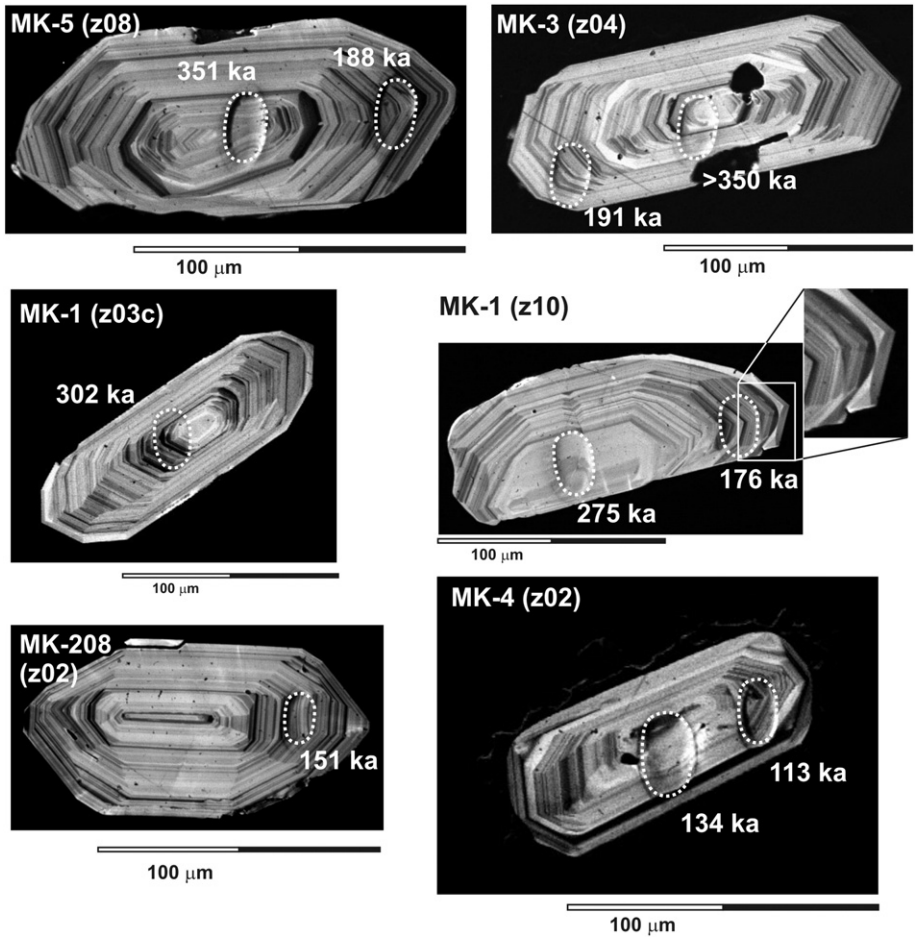

Fig. 4. Cathodoluminescence images of representative zircons from different samples (for zircon grains see Supplementary data) showing the analysed spots and the obtained U-Th and U–Pb (for Mk-1 z03c grain) ages. Note, the resorption surface and zircon overgrowth at the pyramidal faces of the MK-1 zircons.

a positive ion counting detector. A "re-extract" was run after each sample to verify complete outgassing of the crystals. He gas results were corrected for blank, determined by heating individual empty Pt capsules using the same procedure. After laser heating zircon crystals were unwrapped from the Pt capsules, loaded into Savillex Teflon vials, spiked with calibrated ^{233}U and ^{230}Th solutions and dissolved in pressurized bombs using a HF-HNO_3 digestion procedure at 220 °C during 5 days. Sample, blank and spiked standard solutions were analysed for ^{233}U, ^{238}U, ^{230}Th, ^{232}Th, and ^{147}Sm as 0.4 ml solutions using a Perkin Elmer Elan DRC II ICP–MS with an APEX micro-flow nebulizer. Procedural U and Th blanks by this method are usually very stable in a measurement session and below 1.5 pg. Total analytical uncertainty (TAU) was computed as the square root of the sum of the squares of weighted uncertainties of U, Th, Sm and He measurements. The raw (U–Th)/He ages were corrected for alpha ejection (the so-called F_T correction) using the equations and fit parameters given by Farley et al. (1996) and Hourigan et al. (2005). The shape parameters of the crystals were determined by multiple digital microphotographs. The (U–Th)/He ages were calculated by the Taylor Expansion Method (Braun et al., 2012). The TAU and the estimated error of the F_T were used to calculate the uncertainties of F_T-corrected (U–Th)/He ages.

3.4. U–Th ion microprobe analysis

The ^{238}U–^{230}Th disequilibrium dating (hereafter denoted as U–Th dating) was performed by secondary ion mass spectrometry (SIMS) using a CAMECA ims1270 at the University of California Los Angeles following the analysis protocol described by Schmitt et al. (2006). All mounted and polished zircon crystals were coated with a conductive layer of 20–30 nm of Au prior to analysis. Eight to ten crystals per sample were chosen for in-situ analysis (using 25–30 μm spot size) targeting mostly the pyramidal zones on the equatorially polished zircon crystals. Analysis of such spots represents the outermost ca. 1/3 part of the growth zones (and volumetrically the main mass of the crystals). These spots are referred to as zircon 'mantle' analyses, while the spots that were placed in the central part of the polished crystals are termed 'core' analyses. The selection of zircon spot locations was based on the investigation of cathodoluminescence (Fig. 4) and back-scattered images. A subset of zircon grains was also selected for depth profiling measurements ('rim' analyses) where grains were pressed into indium (In) metal with crystal surfaces flush on the surface for ion microprobe analysis without any surface preparation besides ultrasonic cleaning and Au coating. Continuous depth profiling perpendicular to the growth layers to a depth of 4 μm was then preformed to detect the latest time of zircon crystallization before the eruption. The collected data were binned in blocks of five cycles (one depth profiling analysis comprising 30 cycles in total). Accuracy was monitored by interspersed analysis of AS3 zircon standard, which yielded a unity secular equilibrium ratio for $(^{230}Th)/(^{238}U) = 1.022 \pm 0.016$ (activities denoted in parentheses; MSWD = 0.5; n = 8), whereas in the case of the rim-analyses it was $(^{230}Th)/(^{238}U) = 0.981 \pm 0.015$ (MSWD = 2.2; n = 29). U concentrations were estimated from $UO^+/Zr_2O_4^+$ intensity ratios relative to zircon standard 91,500 (U = 81.2 ppm; Wiedenbeck et al., 1995). Crystallization ages were calculated as two-point zircon-melt model isochrons using whole-rock compositions (average Th/U = 3.58) and assuming secular equilibrium of the melt. Because the isochron slope is dominated by the zircon composition, variations in the melt composition within reasonable limits will not significantly change these model ages.

3.5. Luminescence dating

Samples for infrared stimulated luminescence (IRSL) dating were collected by pushing metal tubes horizontally into the previously cleaned near-vertical outcrop wall 20 cm below (202–1) and above (202–3) the contacts to the intercalated tephra bed (MK-202 locality). The preparation of the samples was conducted under subdued red light. A polymineralic fine-grained fraction (4–11 μm) was extracted from the samples by sieving and sequential treatments with 0.1 N hydrochloric acid, 0.01 N sodium-oxalate, and 30% hydrogen peroxide to remove carbonate, clay coating and organic matter from the samples, respectively. Luminescence measurements were performed using an automated Risø TL/OSL-DA-20 reader at the Department of Physical Geography in the Eötvös Loránd University, Institute of Geography and Geology. The reader is equipped with a bialkali EMI 9235QB photomultiplier tube, IR diodes ($\lambda = 875$ nm), blue LEDs ($\lambda = 470$ nm) and a $^{90}Sr/^{90}Y$ β-source. A Schott BG-39 and BG-3 filter package transmitting wavelengths between 350 and 420 nm was placed in front of the photomultiplier to detect the blue light emission for IRSL measurements following the post-IR IRSL 290 protocol (pIRIR290; Thiel et al., 2011). This protocol includes an IR stimulation of 200 s at 50 °C, then an elevated temperature IR stimulation of 200 s at 290 °C. A preheat of 320 °C for 60 s was applied prior to the stimulations. At the end of the measurement cycle an IRSL stimulation at 325 °C for 100 s was performed. The 290 °C stimulation is used to measure the post-IR IRSL signal for the equivalent dose (De) determination. The De values were obtained by integrating the first 2.5 s of the IRSL decay curve and the final 100 s of the stimulation was subtracted to remove the background. Although the pIRIR290 signal of feldspar typically shows negligible fading (Thomsen et al., 2008; Buylaert et al., 2009; Thiel et al., 2011; Buylaert et al., 2012), we performed fading test which resulted in fading rates of 0.64 ± 0.31%/decade for sample 202–1 and 1.5%/decade for the samples 202–3. We consequently applied a fading correction (Huntley and Lamothe, 2001) for 202–3, whereas the fading correction was necessary for 202–1.

Dose rates were obtained from the K, U, and Th content of the bulk sediment as measured by gamma spectrometry in the laboratory at the Leibniz Institute for Applied Geophysics, in Hannover. A potassium content of 12.5 ± 1% (Huntley and Baril, 1997) was applied to the K-rich feldspar fraction to account for the internal dose rate. An average a-value of 0.08 ± 0.02 (Rees-Jones, 1995) was used for the feldspar IRSL age calculation. The cosmic radiation was corrected for altitude and sediment thickness (Prescott and Hutton, 1994), assuming a water content of 15 ± 5% for all samples. Dose rate conversion is based upon the factors of Adamiec and Aitken (1998).

4. Results

4.1. Zircon U–Th dating

The ^{238}U–^{230}Th model ages represent the time of zircon crystallization. They range from 62.6 + 10.7/–9.7 ka to secular equilibrium ≥350 ka (Table 1; see also the Supplementary Table; Fig. 5). When reanalysing secular equilibrium spots using the U–Pb dating technique (see the Supplementary Table) only a single age datum (714 ± 197 ka) was obtained that significantly pre-dates 350 ka, suggesting that zircon crystallization was largely confined to <350 ka or has only slightly older ages (Fig. 6). Zircon ages are thus much younger than the apparent eruption ages indicated by K/Ar and Ar/Ar dating (240–600 ka; Pécskay et al., 1992, 1995; Karátson, 2007; Szakács et al., 2015). On the other hand, zircon crystallization ages in some cases exceed the maximum eruption age estimates (ca. 250 ka) reported in Karátson et al. (2013). This protracted time-span of zircon crystallization is recorded also in individual crystals where analyses on different crystal domains show age differences in excess of 100 ka (Fig. 4). The largest difference was detected in a zircon grain of sample MK-3,

Table 1
Weighted averages of the U–Th ages for 'rim', 'mantle' and 'core' spot analysis of zircons from the Ciomadul samples. Full data set is found in the Supplementary table. Uncertainty values are calculated as 1-sigma error of the weighted averages multiplied by the square root of the MSWD. n is the number of the analyses used in the calculation of the weighted averages. Note, that only those data were considered where the slope of the isochron is <1. The ^{230}Th decay constant used was from Cheng et al. (2013).

Sample	U–Th age	Uncertainty		MSWD	n
	t (ka)	+	−		
Veres-patak (MK-1)					
Rim-analyses (4 μm integrated mean age)	138	13	−12	6.7	13
"Mantle"-spot analyses	141	13	−12	7.5	10
"Core"-spot analyses	194	41	−36	8.2	5
Baile Tusnad (MK-3)					
"Mantle"-spot analyses	136	16	−15	10.1	8
Core spot-analyses	177	47	−43	17.1	5
Mohos east crater rim (MK-4)					
Rim-analyses (4 μm integrated mean age)	134	19	−18	7.6	5
"Mantle"-spot analyses	152	14	−13	7.0	11
Core spot-analyses	202	34	−30	5.9	6
Bükszád roadcut (MK-5)					
Rim-analyses (4 μm integrated mean age)	125	14	−14	13.8	13
"Mantle"-spot analyses	195	15	−14	2.9	10
Târgu Secuiesc (MK-202)					
"Mantle"-spot analyses	147	9	−9	3.0	9
Core spot-analyses	192	44	−38	5.4	3
Kövesponk (MK-208)					
"Mantle"-spot analyses	151	12	−12	3.7	7

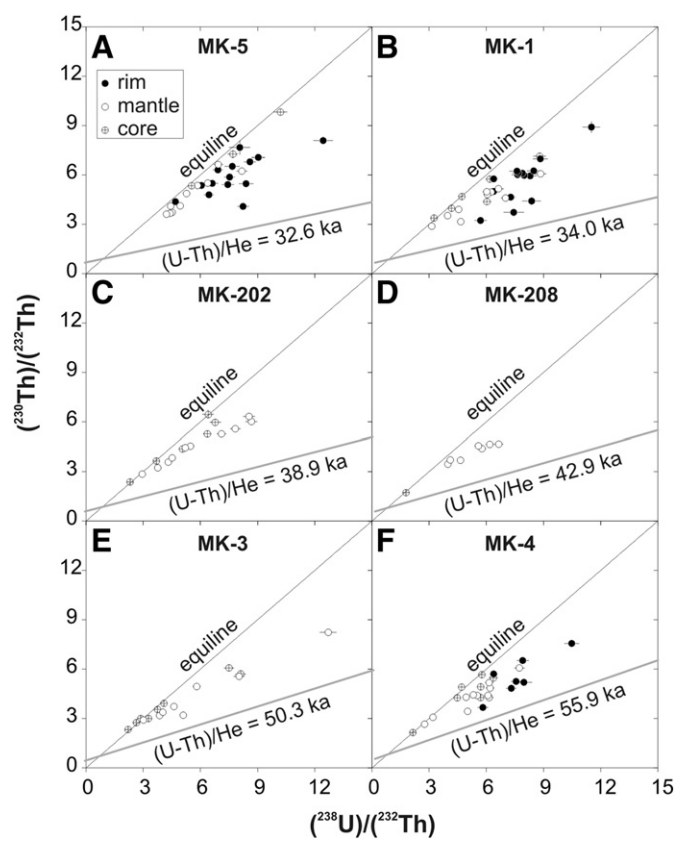

Fig. 5. $^{238}U/^{230}Th$ isochron diagrams showing the "rim" (dark circle), "mantle" (open circle) and core (circle with cross) spot analyses for the studied samples. Isochrons corresponding to the eruption ages obtained from (U–Th)/He zircon dating are indicated; these represent absolute minimum ages for zircon crystallization (i.e., U–Th isotopic compositions must plot between the eruption age isochron and the equiline).

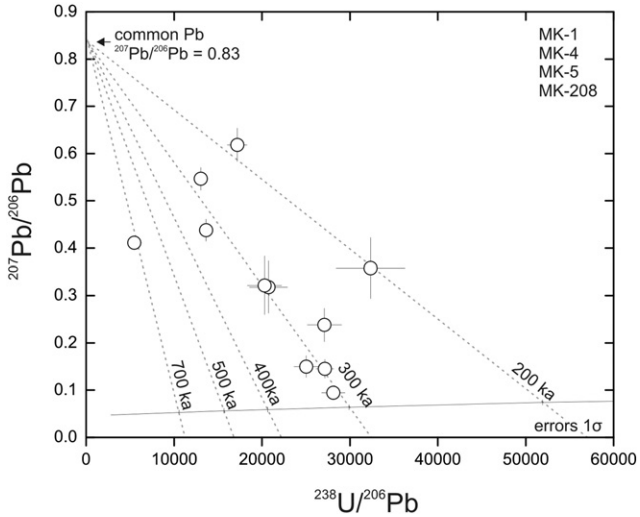

Fig. 6. $^{207}Pb/^{206}Pb$ vs. $^{238}U/^{206}Pb$ diagram for Ciomadul zircons that were determined to be in ^{230}Th-^{238}U secular equilibrium within analytical uncertainties. Data are plotted uncorrected for common Pb with model isochrons between 200 and 700 ka for binary mixing between a radiogenic component and common Pb with $^{207}Pb/^{206}Pb = 0.83$ corresponding to anthropogenic Pb in Southern California (Sañudo-Wilhelmy and Flegal, 1994). Note that Concordia is modified to account for disequilibrium in ^{231} Pa and ^{230}Th for zircon-melt D values of 3 and 0.2, respectively, using equations in Wendt and Carl (1985). Due to the small number of secular equilibrium zircons in the Ciomadul population (n = 11), samples are plotted undifferentiated. With the exception of one datum at ca. 700 ka, all secular equilibrium zircons show U-Pb ages that are between 200 and 300 ka, and are thus concordant with the U–Th results. Data are presented in the Supplementary table.

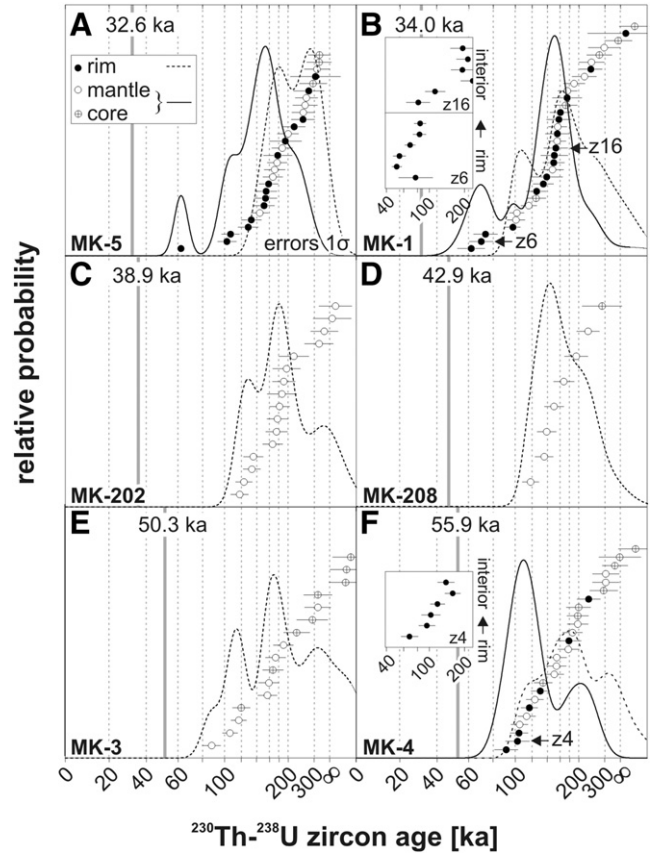

Fig. 7. Zircon crystallization age probability density curves for the studied samples showing the (U-Th)/He zircon ages corrected for U-disequilibrium for comparison. For samples MK-1 (z6 and z16) and MK-4 (z4), insets show depth-profiling results for zircon rims to 4 μm total depth. Ages divided into ~0.67 μm intervals generally increase from the rim (bottom of inset panels) towards the interiors (top); low U in the shallowest depth interval for MK-1 z6 results in a high uncertainty which obscures the age relations for the shallow part of this profile.

where the U–Th date of the crystal core yielded 338 + ∞/−81 ka (∞ indicating secular equilibrium), whereas the age of the 'mantle' domain was determined at 88.4 + 8.9/−8.2 ka. In general, the weighted mean 'core' ages (202–177 ka) are older than that of the 'mantle' domain ages (weighted mean values: 136 ± 16 ka to 152 ± 14 ka, except for the sample MK-5, where the 'mantle' age is 195 ± 15 ka; Fig. 7). The weighted mean 'rim' ages (125 ± 14 ka to 138 ± 13 ka) of most of the samples are indistinguishable within analytical uncertainties from that of the 'mantle' domain ages. The only exception is again sample MK-5, where zircons show significant differences between the 'rim' and 'mantle'-spot ages (125 ± 14 ka and 195 ± 15 ka, respectively). 'Rim' ages are also much older than the eruption age implicated by the ^{14}C charcoal age (31.5 ± 0.3 ka cal BP; Harangi et al., 2010).

Depth profiling ('rim') analysis for most grains reveals homogeneous rim ages (i.e. statistically insignificant age variations along the 4 μm profile), except for a few cases such as in sample MK-4, where the ^{238}U–^{230}Th model ages show a significant increase from 69 + 13/−12 ka to 138 + 25/−20 ka from the outermost rim to 4 μm depth (Fig. 7). The outermost 0.66 μm of a zircon from MK-5 yielded the youngest U–Th age of 48 + 9/−8 ka recorded in any of the dated Ciomadul zircons. This age is, however, still significantly older than the radiocarbon ages for the same deposit.

4.2. Zircon (U–Th)/He ages

(U–Th)/He zircon dating was applied to constrain the eruption ages of the youngest volcanic products of Ciomadul (Table 2 and Fig. 7). The obtained F_T-corrected (U–Th)/He zircon ages prior to correction for disequilibrium range from 113 ka to 24.7 ka, but within this age range, correction for U-series disequilibrium (Farley et al., 2002) is significant. Ciomadul zircons show large and complex U abundance variations from core to rim with differences of up to 2000 ppm. Sector-zoning is a common feature of the crystals (Fig. 4). U-enrichment towards the prism faces is commonly observed, whereas cyclic variations and depletion of the outermost rims in U characterizes many pyramid faces. The heterogeneous distribution of U and Th within individual crystals is biasing the F_T-corrections (Hourigan et al., 2005; Dobson et al., 2008) and can readily explain variations in the (U–Th)/He zircon ages for individual crystals that exceed analytical uncertainties. (U–Th)/He zircon age heterogeneity in distal pumice sample MK-202 between 30.8 and 113 ka, however, exceed the variability that can be reasonably attributed to intra-crystal zonation. Instead, we interpret the older zircon ages as remobilization of crystals from older deposits during the eruption without sufficient heating to reset the (U–Th)/He ages. This is reasonably expected for comparatively low temperatures and rapid cooling in a distal fall-out deposit, whereas magmatic heating would reset He in xenocrystic zircon on the timescales of minutes to days (e.g., Blondes et al., 2007; Cooper et al., 2011). Consequently, we omitted the three oldest zircon ages (60.0, 91.6 and 113 ka) from MK-202 single-grain data for the calculation of the eruption age.

The accurate (U–Th)/He ages require, however, constraints on U-series disequilibria (Farley et al., 2002) which can be garnered from U–Th geochronology. U-series radioactive decay during pre-eruptive crystal residence in the magma chamber reduces the degree of disequilibrium, therefore less correction is needed. In case of relatively homogeneous ^{238}U–^{230}Th model ages consistent with short residence time, the correction is straightforward resulting in well-constrained eruption ages (Gebauer et al., 2014). However, corrections are more difficult when age-zoned zircon crystals are present in the erupted products (e.g., Schmitt et al., 2010b; Danišík et al., 2012) as is the case also for the Ciomadul zircons (Fig. 4). Ciomadul zircons show a wide range of ^{238}U–^{230}Th ages, both in spot analyses of sectioned crystals as well as

Table 2
Results of the (U–Th)/He zircon dating with the uncorrected, F_T–corrected and the disequilibrium-corrected ages. (U–Th)/He ages for the samples are given from the weighted average of the individual corrected (U–Th)/He ages with their uncertainties, the goodness-of-fit parameter and the whole rock U and Th concentrations. * omitted in the calculation of (U-Th)/He eruption age for the sample. Dsq.-cor. =disequlibirum-corrected.

Sample code	^{232}Th (ng)	± (%)	^{238}U (ng)	± (%)	^{4}He (ncc)	± (%)	TAU (%)	Uncorrected (U–Th)/He age (ka)	±2σ (ka)	F_T	F_T–Cor. (U–Th)/He age (ka)	±1σ (ka)	D230	Dsq.-cor. (U–Th)/He age (ka)	+	−
(U–Th)/He age: 34.0 (+1.0, −0.9), n = 8, goodness-of-fit = 0.0396																
Whole-rock U = 3.7 ppm, Th = 15.8 ppm																
MK-1 z1	4.497	2.4	5.696	1.8	0.0217	4.3	4.6	26.6	2.4	0.80	33.40	2.56	0.185	40.8	3.0	3.6
MK-1 z2	4.989	2.4	6.314	1.8	0.0255	4.4	4.6	28.2	2.6	0.81	34.64	2.51	0.185	42.3	2.9	3.7
MK-1 z3	3.813	2.4	5.384	1.8	0.0184	4.9	5.1	24.3	2.5	0.78	31.30	2.64	0.166	38.0	3.7	3.4
MK-1 z4	2.159	2.4	3.816	1.8	0.0110	5.6	5.9	21.1	2.5	0.80	26.18	2.17	0.132	32.0	3.1	2.7
MK-1 z5	3.799	2.4	6.254	1.8	0.0184	4.9	5.2	21.3	2.2	0.81	26.22	2.00	0.142	31.9	2.9	2.4
MK-1 z6	3.939	2.4	4.984	1.8	0.0168	5.4	5.6	23.6	2.6	0.78	30.33	2.64	0.185	36.5	3.6	3.3
MK-1 z7	4.341	2.4	7.310	1.8	0.0208	4.6	4.8	20.6	2.0	0.84	24.68	1.70	0.139	29.7	2.7	1.8
MK-1 z8	13.449	2.4	18.360	1.8	0.0607	2.7	3.1	23.3	1.4	0.87	26.79	1.32	0.172	32.6	1.6	2.1
(U–Th)/He age: 50.3 (+1.3, −1.2), n = 8, goodness-of-fit = 0.0065																
Whole-rock U = 2.9 ppm, Th = 9.5 ppm																
MK-3 z1	9.715	2.4	16.318	1.8	0.0835	2.3	2.8	37.2	2.1	0.86	43.48	2.24	0.182	54.0	3.7	3.5
MK-3 z2	9.260	2.4	14.495	1.8	0.0887	2.0	2.6	44.0	2.2	0.86	51.28	2.54	0.195	63.9	4.6	3.9
MK-3 z3	8.558	2.4	11.534	1.8	0.0601	2.9	3.3	36.7	2.4	0.82	44.61	2.77	0.226	54.2	4.1	3.7
MK-3 z4	6.842	2.4	9.519	1.8	0.0448	3.2	3.5	33.3	2.4	0.84	39.82	2.40	0.219	48.9	2.9	3.8
MK-3 z5	4.600	2.4	7.799	1.8	0.0332	3.7	4.1	31.0	2.5	0.80	38.88	2.85	0.180	47.9	4.4	3.7
MK-3 z6	3.454	2.4	6.418	1.8	0.0293	4.1	4.4	33.5	2.9	0.78	42.74	3.34	0.164	53.4	4.8	4.7
MK-3 z7	15.336	2.4	26.453	1.8	0.1114	2.0	4.1	30.7	2.6	0.86	35.77	2.09	0.177	43.4	3.8	2.3
MK-3 z8	5.861	2.4	9.177	1.8	0.0418	3.2	3.6	32.8	2.4	0.85	38.41	2.17	0.195	47.1	3.2	3.1
(U–Th)/He age: 55.9 (+2.2, −2.3), n = 5, goodness-of-fit = 0.0163																
Whole-rock U = 3.3 ppm, Th = 11.8 ppm																
MK-4 z2	2.094	2.4	3.027	1.8	0.0142	5.6	5.8	33.4	3.9	0.76	43.98	4.08	0.194	53.1	4.7	5.7
MK-4 z3	2.788	2.4	3.861	1.8	0.0228	4.4	4.7	41.8	3.9	0.76	54.98	4.72	0.202	66.4	6.4	6.2
MK-4 z4	5.204	2.4	6.780	1.8	0.0348	3.8	4.1	36.0	2.9	0.79	45.58	3.42	0.215	54.3	4.5	4.5
MK-4 z5	3.216	2.4	5.671	1.8	0.0339	3.9	4.2	43.6	3.7	0.77	56.52	4.54	0.159	69.5	6.7	5.8
MK-4 z6	6.256	2.4	7.336	1.8	0.0338	3.6	3.9	31.8	2.5	0.77	41.11	3.23	0.239	48.5	4.0	4.3
(U–Th)/He age: 32.6 (+1.0, −1.0), n = 5, goodness-of-fit = 0.0013																
Whole-rock U = 3.5 ppm, Th = 14.4 ppm																
MK-5 z1	7.764	2.4	6.584	1.8	0.0233	4.8	5.0	22.9	2.3	0.79	29.02	2.34	0.287	32.0	2.3	2.9
MK-5 z2	5.455	2.4	8.322	1.8	0.0361	3.5	3.8	31.1	2.4	0.83	37.34	2.34	0.159	41.9	2.9	2.7
MK-5 z3	8.827	2.4	13.115	1.8	0.0449	3.1	3.5	24.5	1.7	0.83	29.38	1.79	0.164	33.0	2.1	2.1
MK-5 z4	4.860	2.4	10.360	1.8	0.0284	3.6	4.0	20.5	1.6	0.83	24.75	1.61	0.114	28.0	1.9	1.9
MK-5 z5	5.754	2.4	10.898	1.8	0.0360	3.6	3.9	24.3	1.9	0.83	29.35	1.90	0.128	33.3	2.3	2.3
(U–Th)/He age: 38.9 (+1.6, −1.8), n = 3, goodness-of-fit = 0.206																
Whole-rock U = 3.2 ppm, Th = 11.6 ppm																
MK-202 z1	37.223	2.4	23.601	1.8	0.1224	3.4	3.7	31.3	1.2	0.80	38.96	2.72	0.435	43.7	2.7	3.5
MK-202 z2*	65.273	2.4	44.069	1.8	0.6003	2.5	2.9	83.5	3.3	0.74	112.96	9.40	0.409	137.4	11.2	13.0
MK-202 z3*	12.288	2.4	21.353	1.8	0.1185	4.1	4.4	40.5	0.7	0.67	60.04	6.44	0.159	75.8	8.9	9.5
MK-202 z4	5.148	2.4	7.535	1.8	0.0260	3.8	4.1	24.6	0.4	0.80	30.75	2.22	0.188	37.0	2.5	3.0
MK-202 z5	4.842	2.4	6.490	1.8	0.0221	4.3	4.5	24.0	0.5	0.78	30.78	2.46	0.206	36.6	3.0	3.1
MK-202 z6*	7.534	2.4	8.973	1.8	0.0887	2.7	3.1	68.3	1.5	0.75	91.63	7.55	0.232	118.2	13.1	11.8
(U–Th)/He age: 42.9 (+1.4, −1.5), n = 4, goodness-of-fit = 0.0036																
Whole-rock U = 4.0 ppm, Th = 14.0 ppm																
MK-208 z1	9.861	2.4	12.681	1.8	0.0502	4.6	4.9	27.7	2.7	0.88	31.61	1.93	0.222	37.2	2.3	2.5
MK-208 z2	13.730	2.4	16.794	1.8	0.0867	3.4	3.8	35.8	2.7	0.87	41.28	2.25	0.234	49.1	2.4	3.3
MK-208 z3	7.191	2.4	10.613	1.8	0.0513	4.4	4.6	34.5	3.2	0.84	40.86	2.69	0.194	49.3	3.3	3.7
MK-208 z4	3.910	2.4	7.458	1.8	0.0280	5.8	6.0	27.6	3.3	0.84	33.02	2.55	0.150	39.6	3.5	3.1

in depth profiles, implying long crystallization durations (>100 ka) of individual zircon crystals (Fig. 7). Furthermore, it is noteworthy that even the rim analyses yielded very heterogeneous ^{238}U–^{230}Th model ages, with rim age differences between zircon crystals from the same hand specimen of >150 ka. Thus, careful textural investigation and interpretation of the ^{238}U–^{230}Th zircon data is necessary for the accurate correction of the (U–Th)/He ages. The assumption that the zircon rim crystallization ages being uniform throughout the crystals will result in significant overestimation of (U–Th)/He eruption age when the difference between the zircon core–mantle–rim ages exceed several 10's of ka, as in the case of the Ciomadul zircons.

Correction for U-series disequilibria (Farley et al., 2002) was performed using the MCHeCalc software (Schmitt et al., 2010a) with input parameters of the F_T-corrected (U–Th)/He zircon ages with 1σ uncertainty, D_{230} value (=$[Th/U]_{zircon}/[Th/U]_{bulk\ rock}$) and ^{238}U–^{230}Th model age obtained from the weighted mean ages of the "mantle" spot analyses. Calculation was conducted via Monte-Carlo simulations with 100,000 trials per sample. The eruption age of each sample was determined from the weighted average of the individual corrected (U–Th)/He ages along with their uncertainties (Table 2.). A goodness-of-fit parameter >10^{-4} indicates a uniform age population (Press et al., 2002). The D_{230} value was calculated using individual bulk zircon concentration data and the respective host rock compositions. The pre-eruptive zircon residence time was constrained by the ^{238}U–^{230}Th model ages using the weighted mean ages of the "mantle" spot analyses because the "mantle" parts account for about the 60–65 vol.% of the

entire crystals. Core (representing about 10 vol.% of the zircon crystals) ages are often approaching secular equilibrium whereas the rim ages are either younger or similar to the 'mantle' ages. The deviations of rims and cores from the mantle ages thus are expected to cancel out.

The reliability of these corrections was confirmed for sample MK-5, where well constrained ^{14}C charcoal ages are available (31.5 ± 0.3 ka cal BP; Harangi et al., 2010). Using a 195 ± 15 ka ^{238}U–^{230}Th zircon crystallization model age, we obtained a 32.6 ± 1.0 ka eruption age that agrees with the radiocarbon age within uncertainties. The age of sample MK-5 is the youngest among the studied samples, although the age of the sample MK-1 (34.0 ± 0.9 ka) is very close to it. The distal tephra bed at Târgu Secuiesc (sample MK-202) that is considered to belong to one of the largest explosive eruption events forming the Sf. Ana crater, proved to be significantly older with an age of 38.9 ± 1.7 ka omitting three apparent older (U–Th)/He zircon ages (see above). In contrast, the other pyroclastic fall deposit located closer to the crater (MK-4) shows much older ages (55.9 ± 2.2 ka) and therefore is related to an older explosive eruption. The MK-208 lava dome sample from the margin of the Sf. Ana crater yielded a (U–Th)/He zircon eruption age of 42.9 ± 1.5 ka. In summary, all the studied samples gave eruption ages ranging from ca. 30 to 60 ka.

4.3. Luminescence dating

Luminescence dating for two samples beneath (202–1) and above (202–3) the MK-202 tephra layer at the Târgu Secuiesc locality determined total dose rates of 4.30 ± 0.17 Gy/ka and 3.80 ± 0.17 Gy/ka, respectively. The decay curves of the samples show the typical shape of a feldspar pIRIR290 signal. The pIRIR290 ages are 43.3 ± 3.0 ka for the sample below the tephra bed and 31.4 ± 1.7 ka above it. After fading correction, the age for sample 202–3 increases to 35.9 ± 2.9 ka. These ages closely bracket and justify the disequilibrium corrected (U–Th)/He zircon ages (38.9 ± 1.7 ka) of the intercalated tephra layer (Fig. 8).

5. Discussion

5.1. Determination of eruption ages

(U–Th)/He zircon dating is a powerful tool to determine eruption ages of young volcanic events, particularly when other dating methods such as radiocarbon dating, K/Ar, and $^{40}Ar/^{39}Ar$ techniques encounter analytical or interpretational difficulties often caused by a lack of appropriate materials for dating (e.g., Farley et al., 2002; Schmitt et al., 2010a, 2010b; Danišík et al., 2012; Gebauer et al., 2014; Schmitt et al., 2014). The (U–Th)/He data provide cooling ages for zircon crystals whose closure temperature for He-diffusion is about 150 °C (Farley et al., 2002; Reiners, 2005). For volcanic rocks, these dates thus correspond to the eruption age. A potential caveat is incomplete syn- or post-eruptive resetting of accidental zircon, especially for thin, rapidly cooling pyroclastic deposits. We have identified such grains by their heterogeneous (U–Th)/He ages, and omitted them for eruption age calculation.

The disequilibrium corrected (U–Th)/He data provide the first eruption age constraints for the latest, dominantly explosive stage of volcanism at Ciomadul (Table 2; Fig. 9). The obtained ages are in the range from 32.6 to 55.9 ka. The reliability of these ages was checked by comparison with radiocarbon dating in case of the MK-5 locality and with post-IR IRSL sediment ages in the distal location MK-202. In both cases, we obtained consistent ages that indicate the youngest Ciomadul eruption at 32.6 ± 1.0 ka, whereas the last major explosive eruption which presumably excavated the Sf. Ana crater occurred at 38.9 ± 1.7 ka. The 38.9 ka eruption is classified at least as sub-plinian considering that pumice fragments with 1–6 cm size accumulated in a 20–25 cm thick layer at 22 km distance from the putative vent (Fig. 1B).

Another young eruption age (34.0 ± 0.9 ka; MK-1 sample) for a pumiceous block of a pyroclastic flow deposit north of the Mohos crater is almost indistinguishable within the stated uncertainties from that of MK-5. This implies that the last volcanic activity was characterized by lava dome extrusions accompanied by intermittent collapse episodes (Fig. 9). A related lava dome presently remains unidentified, possibly indicating that all extruded material collapsed and was transformed into pyroclastic flow deposits. The occurrence of charcoal fragments in the pyroclastic flow deposit at the MK-5 locality suggests a high-temperature flow as expected for an explosive lava dome collapse. This assumption is supported also by the pumiceous nature of the blocks in the flow deposit.

The Kövesponk dacite (MK-208) at the southern rim of the Sf. Ana crater is the youngest lava dome dated so far for Ciomadul. The (U–Th)/He dating yielded an age of 42.9 ± 1.5 ka which is significantly younger than the K/Ar age reported elsewhere (290 ± 110 ka; 560 ± 110 ka; Pécskay et al., 1992; Szakács et al., 2015). This young age differs from the other lava dome rocks, where (U–Th)/He ages uncorrected for ^{230}Th–^{238}U disequilibrium suggest >100 ka eruption ages (Karátson

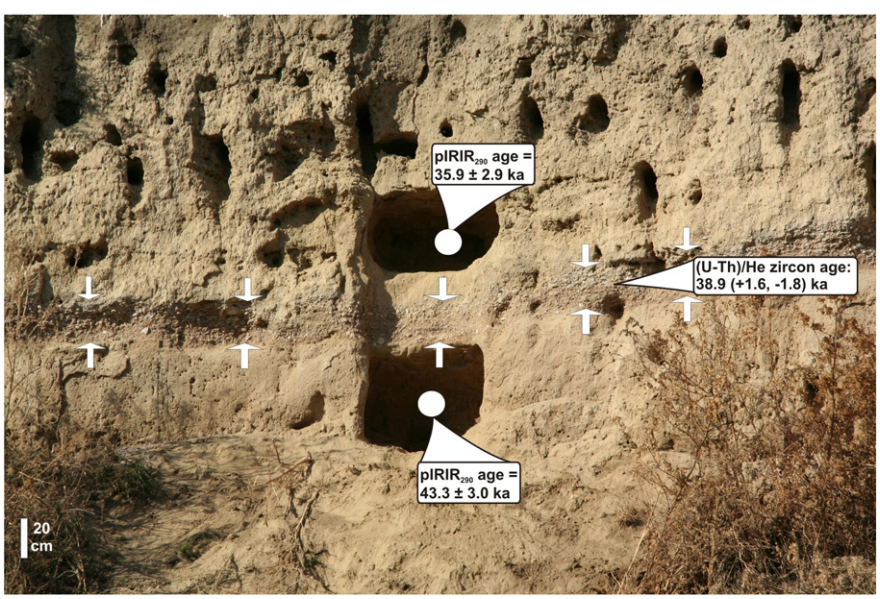

Fig. 8. A 20 cm thick tephra bed in an abandoned sand quarry at Târgu Secuiesc (Kézdivásárhely) 22 km from the Ciomadul (Fig. 1A). The (U-Th)/He zircon age (38.9 ± 1.7 ka) of this distal tephra is confirmed by the infrared stimulated luminescence dating performed for samples taken just beneath (43.3 ± 3.0 ka) and above (35.9 ± 2.9 ka) the tephra bed.

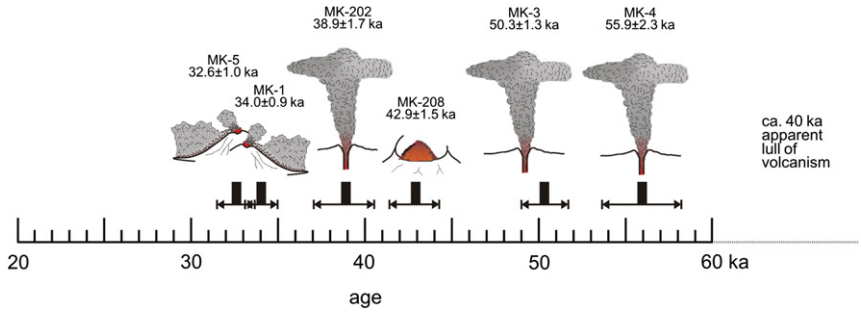

Fig. 9. Schematic illustration of the eruptive history of the youngest, mostly explosive volcanic phase of the Ciomadul with the (U-Th)/He zircon ages.

et al., 2013). On the other hand, this age is very close (within analytical uncertainty) to the 38.9 ± 1.7 ka date obtained for deposits from the explosive eruption which deeply excavated the Sf. Ana crater. The oldest ages within the studied samples were obtained for two pyroclastic fall deposits (MK-3 and MK-4 localities; Fig. 9). The MK-3 sample was collected beneath a massive pyroclastic flow deposit dated at 41.1 ± 0.8 ka cal BP by ^{14}C (Harangi et al., 2010). The MK-3 (U–Th)/He zircon age of 50.3 ± 1.3 ka indicates that the fall-out layer belongs to a significantly older explosive eruption. Large explosive eruptions occurred even before as shown by the (U–Th)/He zircon 55.9 ± 2.3 ka age for a thick (>1.5 m) proximal pumiceous pyroclastic fall deposit, east of the Mohos crater. This crater is considered to be older than Sf. Ana based on the morphological features and the infilling materials which comprise peat-bog in Mohos and a lake in the Sf. Ana craters (Szakács and Seghedi, 1989; Juvigné et al., 1994; Szakács and Seghedi, 1995; Tanţău et al., 2003). We tentatively interpret the 55.9 ka pyroclastic fall deposit to be related to the excavation of the Mohos crater by a subplinian to plinian explosive eruption. Noteworthy, this is the oldest known pyroclastic unit at Ciomadul and is deposited directly on Cretaceous flysch sediments. This suggests that the dominantly explosive volcanic phase of Ciomadul is confined to the 56–32 ka time interval. Furthermore, we emphasize that no eruption ages <32 ka have been obtained by (U–Th)/He zircon (this study) or radiocarbon dating (Vinkler et al., 2007; Harangi et al., 2010). Collectively, these results invalidate a much younger (10.7 ka) age of volcanism as reported by Juvigné et al. (1994) for charcoal fragments of the MK-3 locality.

Noteworthy, the obtained eruption ages are much younger than implied by K–Ar and Ar–Ar dating (>200 ka; Pécskay et al., 1992, 1995; Karátson, 2007; Szakács et al., 2015). Although most of these ages were derived from the older lava dome rocks not discussed here, there are also equivalent results for the same sampling localities as studied here. The most striking differences are reported ages for the Kövesponk lava dome. Pécskay et al. (1992) and Szakács et al. (2015) published 560 ± 110 ka and 290 ± 110 ka ages using the K/Ar dating technique on separated biotite. Based on these results, they considered Kövesponk as one of the oldest lava domes at Ciomadul. In contrast, our combined U–Th and (U–Th)/He zircon dating (zircon crystallization and eruption ages, respectively) clearly suggests that it is much younger (118–300 ka zircon crystallization age and 42.9 ± 1.5 ka eruption age) and, in fact, the youngest known lava dome for Ciomadul. Karátson (2007) reported Ar–Ar ages for biotites separated from pumice collected in localities MK-1 and MK-3. An age of 479 ± 49 ka was determined for the massive pyroclastic rock, which overlies the pyroclastic fall layer (sample MK-3) for which the combined U–Th and (U–Th)/He methods yielded 50.3 ± 1.3 ka. At the MK-1 locality, pumices from a pyroclastic fall layer overlying the pyroclastic flow deposit dated here (34.0 ± 0.9 ka) yielded an Ar–Ar biotite age of 270 ± 20 ka. This Ar–Ar age is unreasonably old compared to both, the U–Th zircon crystallization (youngest ages between 66 ka and 80 ka) and (U–Th)/He zircon eruption ages. We thus interpret the too old Ar–Ar biotite ages to reflect excess ^{40}Ar (e.g., Hora et al., 2010). Based on our new results on the eruption dates a reconsideration is required for the volcanic evolution of Ciomadul volcano and the nearby dacitic lava domes (Szakács et al., 2015). Further combined U–Th and (U–Th)/He zircon dating would be particularly helpful in this study.

The eruption age of the MK-1 sample also constrains the time of formation of the lake within the Mohos crater. A succession of intercalated lacustrine sand beds with pumiceous layers above the pyroclastic flow deposit was dated by Karátson (2007) to define the onset of lake formation within the crater. The 34.0 ± 0.9 ka (U–Th)/He zircon eruption age of the pyroclastic flow deposit provides a maximum age for the appearance of lacustrine deposits within the crater, although the formation of the explosion crater could possibly go back as far as the deposition age of the MK-4 pyroclastic fall-out layer at 55.9 ± 2.3 ka.

5.2. Significance of the eruption dates in a tephrochronologic context

During the last 100 ka, volcanism in continental Europe occurred in northeastern Spain (Garrotxa, Martí et al., 2011; Puiguriguer et al., 2012), in the Massif Central in central France (Nowell et al., 2006; Chapron et al., 2010) and in the Eifel region of western Germany (van den Bogaard, 1995; Schmitt, 2006; Schmincke, 2007) in addition to abundant volcanic activity in Italy and Greece (Fig. 10). Large explosive eruptions during this time interval produced widespread tephras covering significant parts of Europe, including the vast Laacher See eruption from the Eifel (12.9 ka; van den Bogaard, 1995) and to a lesser extent the Chopin, Kilian, and Vasset centres in the Chaine des Puys, Massif Central (Juvigné, 1992; Juvigné et al., 1992; Vernet and Raynal, 2008). Furthermore, several large eruptions occurred in central Italy such as the Campanian Ignimbrite at ca. 40 ka and the Neapolitan Yellow Tuff at ca. 14 ka from Campi Flegrei, and the Codola Tuff from Vesuvius at ca. 33 ka (De Vivo et al., 2001; Di Vito et al., 2008; Santacroce et al., 2008; Gebauer et al., 2014). Quaternary volcanic activity in eastern–central Europe is, however, much less known. Our zircon dating of the Ciomadul dacites provides age constraints on its latest, mostly explosive eruptions, which took place between 56 and 32 ka. These results have broad significance for tephrochronologic studies in the eastern–central and south–eastern Europe (e.g., Schmidt et al., 2002; Pyle et al., 2006; Caron et al., 2010; Vogel et al., 2010; Lane et al., 2011; Morley and Woodward, 2011; Lane et al., 2012; Veres et al., 2013; Cullen et al., 2014). There are many lake sediments in this part of Europe where distal tephra deposits originating from major explosive eruptions from Ciomadul could be potentially preserved. Conventionally, most distal tephras in this region are regarded to be derived from eruptions within central Italy during the last 100 ka (e.g., Calanchi and Dinelli, 2008; Bourne et al., 2010; Morley and Woodward, 2011), mainly the ca. 40 ka Y5 tephra of the Campanian Ignimbrite eruption, the ca. 33 ka Codola tephra from Vesuvius and the ca. 30–31 ka Y3 tephra from Campi Flegrei.

The time span of these tephras sourced from central Italian volcanoes overlaps the latest volcanic eruption stage (56–32 ka) of Ciomadul volcano. A distal pumiceous bed located 22 km southeast of Ciomadul indicates a relatively large, possibly subplinian–plinian eruption (Szakács and Seghedi, 2013). We dated this deposit at 38.9 ± 1.7 ka, which overlaps with the eruption age of the Campanian Ignimbrite

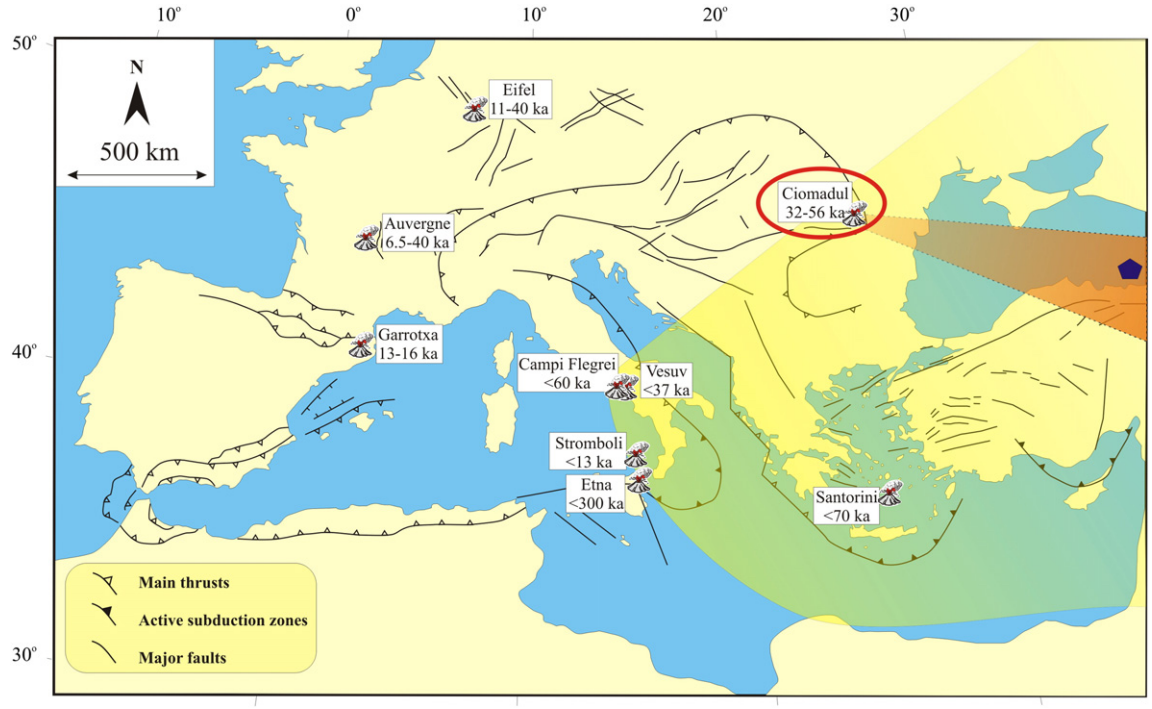

Fig. 10. Map showing the <100 ka volcanic eruption sites in Europe. Presumed dispersion axis of the 38.9 ka tephra of Ciomadul overlaps that of the coeval Campanian Ignimbrite tephra (Pyle et al., 2006). Location of the M72/5-25-GC1 drilling core at the southern part of the Black Sea (Cullen et al., 2014) is also indicated.

within uncertainty. Tephra deposits of the Campanian Ignimbrite eruption are found at many localities over southeast Europe as far as to Moscow (Pyle et al., 2006; Veres et al., 2013; Fitzsimmons et al., 2013; Cullen et al., 2014). The presumed dispersion axis of the tephra of the large 38.9 ka Ciomadul eruption crosses that of the Campanian Ignimbrite tephra in the Black Sea region (Fig. 10). Cullen et al. (2014) reported 22 volcanic glass horizons in a core from the southeast Black Sea and they cover the last 60 ka. The origins of many of these tephra beds are unknown, particularly in the time range between 34–38 ka and 40–48 ka (Cullen et al., 2014). Cullen et al. (2014) suspected that Ciomadul could be a possible candidate for these tephras. The major element compositions of these distal tephra glasses are rhyolitic, as are the Ciomadul pyroclastic deposits (Vinkler et al., 2007). Although major elements are not sufficiently discriminative, we suspect that the abundances of Ba and Sr and characteristic depletions of heavy rare earth elements in the Ciomadul dacites (Vinkler et al., 2007) would reliably fingerprint Ciomadul tephra in distal deposits.

5.3. Implications for magma chamber processes and magma residence time

The U–Th model ages of Ciomadul zircons show a wide range, even at the intra-crystal scale, reflecting prolonged crystallization in a crustal magma chamber. The oldest zircon crystallization ages of ca. 300–350 ka are near secular equilibrium, and thus poorly constrained. U–Pb zircon dating suggests, however, that these zircons are not much older than the ca. 300–350 ka U–Th ages. Noteworthy, the (U–Th)/He data of the oldest lava domes are in the range of 80–140 ka (Karátson et al., 2013) indicating that the peak of the lava dome building phase occurred between ca. 100 and 150 ka (Fig. 11). This is much younger than suggested by published K/Ar and Ar/Ar data (Pécskay et al., 1992, 1995; Karátson, 2007), although the (U–Th)/He data in Karátson et al. (2013) are minimum ages because they are not corrected for U-series disequilibrium. (U–Th)/He eruption ages >150 ka are so far lacking for Ciomadul. The crystallization of zircon and the development of a crustal magma storage therefore could have preceded the onset of the volcanic activity possibly by >100 ka (Fig. 11). Such long crystal residence is not unprecedented. Protracted zircon crystallization has been documented for silicic magma systems in various tectonic environments (Reid et al., 1997), including multiple volcanic centres located in continental (e.g., Bacon and Lowenstern, 2005; Claiborne et al., 2010; Klemetti and Clynne, 2014) and oceanic arcs (Schmitt et al., 2010b), albeit with the difference that these magma systems frequently vented resulting in volcanic eruptions, whereas we have currently no evidence for eruptions >150 ka at Ciomadul considering the (U–Th)/He data published here and the uncorrected age data described in Karátson et al. (2013). However, there are also examples where U–Th zircon ages are homogeneous or with negligible age differences, especially in basalt-dominated or alkaline systems (e.g., Schmitt et al., 2011; Gebauer et al., 2014).

Amphibole-plagioclase thermometry suggests that a low temperature (700–750 °C) magma reservoir existed beneath Ciomadul before the eruptions where injection of hot basaltic magma (as evident from xenocrystic mineral assemblages in the dacites including olivine and clinopyroxene; Harangi et al., 2015) into the crystal-rich mush mobilized the felsic magma and rapidly triggered eruptions (Kiss et al., 2014). Effective reactivation requires that the melt content in the magma reservoir increases to >60% (Bachmann and Bergantz, 2004; Huber et al., 2011) allowing eruptible magma to coalesce. Thermometry calculation implies heating >200 °C beneath Ciomadul briefly before the eruptions (Kiss et al., 2014; Harangi et al., 2015). After withdrawal of the eruptible portion of magma along with parts of the crystal mush, the system cooled and hibernated in a mushy state for a prolonged period until a new magma influx occurred. Because of the comparatively low zircon saturation temperatures (700–760 °C for Ciomadul whole rock; 780–800 °C for pumice glass; using the calibration in Boehnke et al., 2013), zircon is associated with cooling and low-temperature storage in the silicic crystal mush body along with a low-temperature paragenesis comprising quartz, plagioclase, K-feldspar, low-Al amphibole, biotite, titanite and apatite (e.g., "cold storage" in Cooper and Kent, 2014). The zircon crystallization age spectra of the youngest (ca. 56–32 ka) volcanic rocks of Ciomadul range over 300 ka and are thus prima facie evidence for a long-lasting mushy magmatic body beneath the volcano. Furthermore, zircon crystallization age spectra indicate a long construction period of this subterraneous magma system

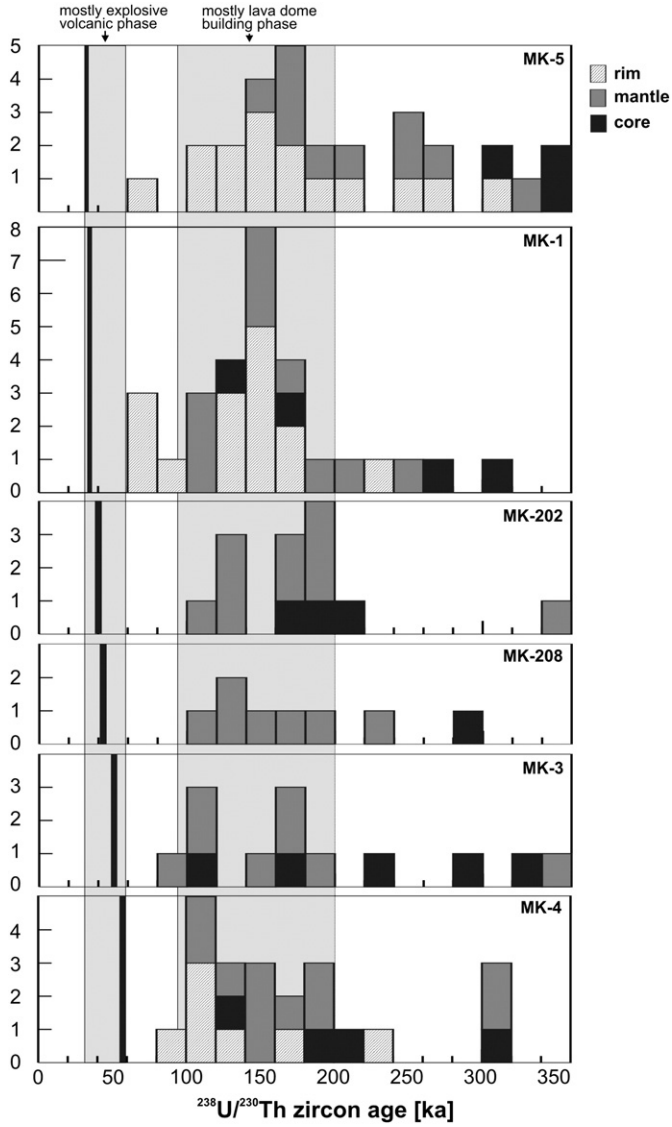

Fig. 11. Zircon U-Th model age distributions for the studied samples. The culmination of the crystallization ages overlaps the onset of the volcanic activity of Ciomadul at around 100–200 ka. Note, that crystallization of zircons started >100 ka before the main lava dome eruption phase and none of the "rim" ages reaches the eruption dates (denoted by solid lines).

for about 100–150 ka before the onset of any known volcanic eruptions. The continuous age distribution of the zircon core to rim analyses from 350 ka to 100 ka, as well as the large age ranges in individual crystals (e.g., 340–88 ka and the 350–191 ka core–rim ages of the MK3_03 and MK5_08 zircon grains, respectively; Fig. 4) imply a long-lived magma system which can be explained by regular influx of mafic magma keeping the mushy magma reservoir continuously partially molten (Reid et al., 1997). The peak zircon crystallization ages fall between 200 and 100 ka, which defines a dominant and overlapping mode in all samples (Fig. 11). This time interval is consistent with the presumed onset of Ciomadul volcanic activity and indicates that conditions were partially favourable for zircon crystallization in the magma reservoir even during rejuvenation periods of an active volcanic phase.

Felsic crystal clots and mineral assemblages (Kiss et al., 2014) in all samples suggest that conditions of cold magma storage prevailed during the entire lifetime of Ciomadul volcano. However, it is noteworthy that for rocks erupted between 56 and 32 ka, zircons with >100 ka crystallization ages dominate and evidence for zircon crystallization close to the time of eruption is lacking. Thus, these zircons are entirely antecrysts (Bacon and Lowenstern, 2005; Miller et al., 2007), and no autocryst or autocrystic domains exist. The paucity of zircon crystallization immediately predating eruption has been documented before (Reid et al., 1997; Claiborne et al., 2010; Schmitt et al., 2010b; Stelten and Cooper, 2012; Klemetti and Clynne, 2014), although there are other examples where zircon crystallization occurred even shortly before eruption (Charlier et al., 2005; Bachmann et al., 2007; Gebauer et al., 2014). The lack of young zircons in the Ciomadul magma and possibly elsewhere could be due to hot mafic magma injection leading to remelting of a comparatively cold silicic crystal mush where the melt is initially zircon saturated but then becomes undersaturated upon heating and/or magma mixing. Under these conditions, zircons suspended in the melt will not crystallize, but rather resorb. In fact, Ciomadul zircon crystals with resorbed margins exist, although the majority of crystals is either euhedral or shows only slight rounding of the pyramid faces. Preservation of zircons even in the groundmass of pumice and lava reinforces a rapid (<100 a) rejuvenation of relatively small to medium silicic magmatic systems (e.g., Burgisser and Bergantz, 2011; Cooper and Kent, 2014). During such timescales only the outermost parts of the zircons can become resorbed which would explain the lack of zircon dating to <10's of ka before eruption. On the other hand, each rejuvenation event could strongly mix the magma reservoir allowing collection of zircons formed at various stages of magma evolution. This is reflected by the distinct rim ages of zircons in individual samples.

Diverse rim ages can also result from shielding zircons from dissolution for prolonged periods. Petrographic observations suggest that zircon crystals occur frequently as inclusions in various minerals forming felsic crystal clots, mostly in plagioclase. Thus, the variation in rim ages may indicate that zircon crystals formed in different parts of the magma body and their crystallization stopped at different times, either because some parts of the magma system cooled rapidly below subsolidus temperatures (Schmitt et al., 2010b), or zircon crystals became embedded in the growing phenocrysts, such as plagioclase or biotite and thus were armoured from resorption once the magma reheated and locally turned zircon undersaturated. Multiple resorption and overgrowth episodes are evident in some crystals as truncated oscillatory growth banding (e.g., MK-1; Fig. 4), suggesting that the melt alternated between zircon saturation and undersaturation. Preliminary microprobe data indicate a significant drop of Hf abundances in the overgrowth layer, consistent with the presence of less evolved and possibly higher temperature melts. Where dated, these resorption-overgrowth features are entirely >50 ka and thus likely unrelated to the ultimate reheating event which triggered eruption at 34.0 ± 0.9 ka. It may, however, correspond to an earlier thermal rejuvenation episode after which residual zircon crystals became embedded in phenocrysts crystallizing during subsequent cooling.

Besides zircon, there is additional evidence for the presence of a melt-bearing crystal mush body beneath Ciomadul with the potential for fast rejuvenation by injection of hot basaltic magma into the cold storage. Seismic (Popa et al., 2012) and magnetotelluric data (Harangi et al., 2015), strong CO_2 emanations often accompanied with release of H_2S and SO_2, and relatively high $^3He/^4He$ isotope ratios of natural gases and CO_2-rich mineral waters (Althaus et al., 2000; Vaselli et al., 2002) are consistent with a melt-bearing magmatic body presently existing in the crust beneath Ciomadul. The new geochronologic data presented here confirms that such long-lasting, low-temperature magma storage could be reactivated even after they resided in their storage reservoir for several 10's of ka. Thus, collective evidence from geology, petrology, and geophysics underscores that Ciomadul should be regarded as a volcano with "Potentially Active Magma Storage" (PAMS; Harangi et al., 2015) in future hazard assessments.

6. Conclusions

1. High-spatial resolution in-situ zircon geochronology constrains the timescales of volcanic eruptions of the youngest, mostly explosive volcanic phase of the Ciomadul volcano, located at eastern–central

Europe. Published ^{14}C charcoal ages (Moriya et al., 1996; Vinkler et al., 2007; Harangi et al., 2010) indicated that volcanic eruptions occurred as young as 31.5 ka, but no information existed on the ages of other young eruptions. (U–Th)/He dating combined with ^{238}U–^{230}Th crystallization ages was used here to refine these eruption ages revealing a sequence of repeated, mostly explosive volcanic eruptions between 55.9 ± 2.3 ka and 32.6 ± 1.0 ka. The reliability of these eruption ages is established by concordant ages obtained from different dating techniques, such as zircon geochronology combined with radiocarbon and infrared stimulated luminescence dating for the same deposits. Thus, relatively young (<60 ka), voluminous volcanism existed in eastern–central Europe. Furthermore, considering all the available (U–Th)/He zircon ages published here and in Karátson et al. (2013), volcanism at Ciomadul must be considered as much younger and with more rapid recurrence within a briefer time period than previously thought (e.g., Pécskay et al., 1992, 1995; Karátson, 2007; Szakács et al., 2015). This requires a reconsideration of magma-flux rates for the region.

2. Within the youngest volcanic phase of Ciomadul, at least four major eruptive episodes can be distinguished. Among them, relatively large (sub-plinian to plinian) explosive eruptions produced distal tephras covering extended areas mostly southeast of the volcano. One of these explosive eruptions dated at 38.9 ka by (U–Th)/He zircon analysis overlaps the age of the Campanian Ignimbrite eruption within uncertainty. The nearly coeval Ciomadul and Campanian Ignimbrite eruptions both have overlapping tephra dispersion axes in southeastern Europe. However, the distinct trace element fingerprint of the Ciomadul volcanic products (Vinkler et al., 2007) compared to central Italian sources could help in the identification of the Ciomadul glass shards in lake sediments.
3. The wide range of U–Th model ages of the studied zircons indicates prolonged existence of a low-temperature (<800 °C) silicic crystal mush beneath Ciomadul. The main zircon crystallization period was between ca. 100 and 200 ka, coeval with the older, mostly extrusive lava dome building stage of Ciomadul volcanism. The lack of zircon rims with crystallization ages closely approaching the eruption age possibly implies re-heating above zircon saturation temperatures by injection of mafic magmas, which is also inferred from amphibole-plagioclase thermometry (>200 °C increase in temperature; Kiss et al., 2014).
4. The diversity of zircon ages in Ciomadul dacites is similar to that of continental and oceanic arc volcanic centres such as Mt. St. Helens (Claiborne et al., 2010), Soufrière/St. Lucia (Schmitt et al., 2010b), and the Lassen Volcanic Complex (Klemetti and Clynne, 2014), where partial rejuvenation of a cold magma storage zone by intrusion of hot mafic magma played a significant role in triggering eruptions and possibly also keeping the intrusive magmatic reservoir in a partially melted state.
5. Rejuvenation of the cold magmatic storage is considered to be a fast process (<100 a) and can occur intermittently if a melt-bearing crystal mush exists beneath the volcano. A melt-bearing magmatic body is inferred to be present beneath Ciomadul at 5–20 km depth which can be rejuvenated via mafic magma injection. Thus, we classify Ciomadul as a typical volcano associated with 'Potentially Active Magma Storage' (PAMS).

Supplementary data to this article can be found online at http://dx.doi.org/10.1016/j.jvolgeores.2015.05.002.

Acknowledgements

The initial part of this research on the Ciomadul volcano belonged to the scientific project supported by the OTKA (Hungarian National Research Fund) No. K68587, whereas the zircon geochronological studies were supported by the Hungarian Academy of Science Research Group project. The infrared stimulated luminescence dating is part of the OTKA project No. 100315. The GATAN MiniCL facility belongs to the KMOP project nr. 4.2.1/B-10-2011-0002 by the European Union. Participation of the young scientists, Balázs Kiss and Réka Lukács in this research was supported by the European Union and the State of Hungary, co-financed by the European Social Fund in the framework of TÁMOP-4.2.4.A/2-11/1-2012-0001 'National Excellence Program'. Réka Lukács's research was supported by the Bolyai János Fellowship. The ion microprobe facility at UCLA is partly supported by a grant from the Instrumentation and Facilities Program, Division of Earth Sciences, National Science Foundation. S.I. benefited by a grant of the Ministry of National Education, CNCS — UEFISCDI, project number PN-II-ID-PCE-2012-4-0137. We thank Cornelius Fischer (Bremen) for the depth-profiling of the ion microprobe craters and the LIAG (Hannover) for the dosimetry measurements. Csaba Jánosi provided invaluable help in the field work what is very much appreciated. Constructive review provided by Jorge Vazquez helped to improve our manuscript. Diligent editorial handling by Malcolm Rutherford is appreciated.

References

Adamiec, G., Aitken, M., 1998. Dose rate conversion factors: update. Ancient TL 16, 37–50.
Althaus, T., Niedermann, S., Erzinger, J., 2000. Noble gas studies of fluids and gas exhalations in the East Carpathians, Romania. Chem. Erde 60, 189–207.
Bachmann, O., Bergantz, G.W., 2004. On the origin of crystal-poor rhyolites: extracted from batholithic crystal mushes. J. Petrol. 45, 1565–1582.
Bachmann, O., Charlier, B.L.A., Lowenstern, J.B., 2007. Zircon crystallization and recycling in the magma chamber of the rhyolitic Kos Plateau Tuff (Aegean arc). Geology 35, 73–76.
Bacon, C.R., Lowenstern, J.B., 2005. Late Pleistocene granodiorite source for recycled zircon and phenocrysts in rhyodacite lava at Crater Lake, Oregon. Earth Planet. Sci. Lett. 233, 277–293.
Blondes, M.S., Reiners, P.W., Edwards, B.R., Biscontini, A., 2007. Dating young basalt eruptions by (U–Th)/He on xenolithic zircons. Geology 35 (1), 17–20.
Boehnke, P., Watson, E.B., Trail, D., Harrison, T.M., Schmitt, A.K., 2013. Zircon saturation revisited. Chem. Geol. 351, 324–334.
Bourne, A.J., Lowe, J.J., Trincardi, F., Asioli, A., Blockley, S.P.E., Wulf, S., Matthews, I.P., Piva, A., Vigliotti, L., 2010. Distal tephra record for the last ca 105,000 years from core PRAD 1–2 in the central Adriatic Sea: implications for marine tephrostratigraphy. Quat. Sci. Rev. 29, 3079–3094.
Braun, J., van der Beek, P., Batt, G., 2012. Quantitative Thermochronology — Numerical Methods for the Interpretation of Thermochronological Data. Cambridge Univ. Press (272 pp.).
Burgisser, A., Bergantz, G.W., 2011. A rapid mechanism to remobilize and homogenize highly crystalline magma bodies. Nature 471, 212–215.
Buylaert, J.-P., Jain, M., Murray, A.S., Thomsen, K.J., Jain, M., 2009. Testing the potential of an elevated temperature IRSL signal from K-feldspar. Radiat. Meas. 44, 560–565.
Buylaert, J.-P., Jain, M., Murray, A.S., Thomsen, K.J., Thiel, C., Sohbati, R., 2012. A robust feldspar luminescence dating method for Middle and Late Pleistocene sediments. Boreas 41, 435–451.
Calanchi, N., Dinelli, E., 2008. Tephrostratigraphy of the last 170 ka in sedimentary successions from the Adriatic Sea. J. Volcanol. Geotherm. Res. 177, 81–95.
Caron, B., Sulpizio, R., Zanchetta, G., Siani, G., Santacroce, R., 2010. The Late Holocene to Pleistocene tephrostratigraphic record of Lake Ohrid (Albania). C. R. Geosci. 342, 453–466.
Chapron, E., Albéric, P., Jézéquel, D., Versteeg, W., Bourdier, J.-L., Sitbon, J., 2010. Multidisciplinary characterisation of sedimentary processes in a recent maar lake (Lake Pavin, French Massif Central) and implication for natural hazards. Nat. Hazards Earth Syst. Sci. 10, 1815–1827.
Charlier, B.L.A., Wilson, C.J.N., Lowenstern, J.B., Blake, S., Van Calsteren, P.W., Davidson, J.P., 2005. Magma generation at a large, hyperactive silicic volcano (Taupo, New Zealand) revealed by U–Th and U–Pb systematics in zircons. J. Petrol. 46, 3–32.
Cheng, H., Edwards, R.L., Shen, C.C., Polyak, V.J., Asmerom, Y., Woodhead, J., Hellstrom, J., Wang, Y., Kong, X., Spötl, C., Wang, X., Alexander, E.C., 2013. Improvements in ^{230}Th dating, ^{230}Th and ^{234}U half-life values, and U–Th isotopic measurements by multi-collector inductively coupled plasma mass spectrometry. Earth Planet. Sci. Lett. 371, 82–91.
Claiborne, L.L., Miller, C.F., Flanagan, D.M., Clynne, M.A., Wooden, J.L., 2010. Zircon reveals protracted magma storage and recycling beneath Mount St. Helens. Geology 38, 1011–1014.
Cloetingh, S.A.P.L., Burov, E., Matenco, L., Toussaint, G., Bertotti, G., Andriessen, P.A.M., Wortel, M.J.R., Spakman, W., 2004. Thermo-mechanical controls on the mode of continental collision in the SE Carpathians (Romania). Earth Planet. Sci. Lett. 218, 57–76.
Cooper, K.M., Kent, A.J.R., 2014. Rapid remobilization of magmatic crystals kept in cold storage. Nature 506, 480–483.
Cooper, F.J., van Soest, M.C., Hodges, K.V., 2011. Detrital zircon and apatite (U-Th)/He geochronology of intercalated baked sediments: a new approach to dating young basalt flows. Geochem. Geophys. Geosyst. 12, Q07003.
Cullen, V.L., Smith, V.C., Arz, H.W., 2014. The detailed tephrostratigraphy of a core from the south-east Black Sea spanning the last ~ 60 ka. J. Quat. Sci. 29, 675–690.

Danišík, M., Shane, P., Schmitt, A.K., Hogg, A., Santos, G.M., Storm, S., Evans, N.J., Fifield, L.K., Lindsay, J.M., 2012. Re-anchoring the late Pleistocene tephrochronology of New Zealand based on concordant radiocarbon ages and combined $^{238}U/^{230}Th$ disequilibrium and (U–Th)/He zircon ages. Earth Planet. Sci. Lett. 349, 240–250.

de Vivo, B., Rolandi, G., Gans, P.B., Calvert, A., Bohrson, W.A., Spera, F.J., Belkin, H.E., 2001. New constraints on the pyroclastic eruptive history of the Campanian volcanic plain (Italy). Mineral. Petrol. 73, 47–65.

Di Vito, M.A., Sulpizio, R., Zanchetta, G., D'Orazio, M., 2008. The late Pleistocene pyroclastic deposits of the Campanian plain: new insights into the explosive activity of Neapolitan volcanoes. J. Volcanol. Geotherm. Res. 177, 19–48.

Dobson, K.J., Stuart, F.M., Dempster, T.J., 2008. U and Th zonation in Fish Canyon Tuff zircons: implications for a zircon (U–Th)/He standard. Geochim. Cosmochim. Acta 72, 4745–4755.

Downes, H., Seghedi, I., Szakács, A., Dobosi, G., James, D.E., Vaselli, O., Rigby, I.J., Ingram, G.A., Rex, D., Pécskay, Z., 1995. Petrology and geochemistry of the late Tertiary/Quaternary mafic alkaline volcanism in Romania. Lithos 35, 65–81.

Farley, K.A., Wolf, R., Silver, L., 1996. The effects of long alpha-stopping distances on (U–Th)/He ages. Geochim. Cosmochim. Acta 60, 4223–4229.

Farley, K.A., Kohn, B.P., Pillans, B., 2002. The effects of secular disequilibrium on (U–Th)/He systematics and dating of Quaternary volcanic zircon and apatite. Earth Planet. Sci. Lett. 201, 117–125.

Fillerup, M.A., Knapp, J.H., Knapp, C.C., Raileanu, V., 2010. Mantle earthquakes in the absence of subduction? Continental delamination in the Romanian Carpathians. Lithosphere 2, 333–340.

Fitzsimmons, K.E., Hambach, U., Veres, D., Iovita, R., 2013. The Campanian Ignimbrite eruption: new data on volcanic ash dispersal and its potential impact on human evolution. PLoS ONE 8, e65839.

Gebauer, S., Schmitt, A.K., Pappalardo, L., Stockli, D.F., Lovera, O.M., 2014. Crystallization and eruption ages of Breccia Museo (Campi Flegrei Caldera, Italy) plutonic clasts and their relation to the Campanian Ignimbrite. Contrib. Mineral. Petrol. 167. http://dx.doi.org/10.1007/s00410-013-0953-7.

Harangi, S., 2001. Neogene to Quaternary volcanism of the Carpathian–Pannonian Region — a review. Acta Geol. Hung. 44, 223–258.

Harangi, S., Lenkey, L., 2007. Genesis of the Neogene to Quaternary volcanism in the Carpathian–Pannonian region: role of subduction, extension, and mantle plume. Geol. Soc. Am. Spec. Pap. 418, 67–92.

Harangi, Sz, Molnár, M., Vinkler, A.P., Kiss, B., Jull, A.J.T., Leonard, A.E., 2010. Radiocarbon dating of the last volcanic eruptions of Ciomadul volcano, Southeast Carpathians, eastern–central Europe. Radiocarbon 52, 1498–1507.

Harangi, S., Sági, T., Seghedi, I., Ntaflos, T., 2013. A combined whole-rock and mineral-scale investigation to reveal the origin of the basaltic magmas of the Perşani monogenetic volcanic field, Romania, eastern–central Europe. Lithos 180–181, 43–57.

Harangi, S., Novák, A., Kiss, B., Seghedi, I., Lukács, R., Szarka, L., Wesztergom, V., Metwaly, M., Gribovszki, K., 2015. Combined magnetotelluric and petrologic constrains for the nature of the magma storage system beneath the Late Pleistocene Ciomadul volcano (SE Carpathians). J. Volcanol. Geotherm. Res. 290, 82–96.

Hora, J.M., Singer, B.B., Wörner, G., 2010. Volcano evolution and eruptive flux on the thick crust of the Andean Central Volcanic Zone: $^{40}Ar/^{39}Ar$ constraints from Volcán Parinacota, Chile. Geol. Soc. Am. Bull. 119, 343–362.

Hourigan, J.K., Reiners, P.W., Brandon, M.T., 2005. U–Th zonation-dependent alpha-ejection in (U–Th)/He chronometry. Geochim. Cosmochim. Acta 69, 3349–3365.

Huber, C., Bachmann, O., Dufek, J., 2011. Thermo-mechanical reactivation of locked crystal mushes: melting-induced internal fracturation and assimilation processes in magmas. Earth Planet. Sci. Lett. 304, 443–454.

Huntley, D.J., Baril, M.R., 1997. The K content of the K-feldspars being measured in optical dating or in thermoluminescence dating. Ancient TL 15, 11–13.

Huntley, D.J., Lamothe, M., 2001. Ubiquity of anomalous fading in K-feldspars, and the measurement and correction for it in optical dating. Can. J. Earth Sci. 38, 1093–1106.

Ismail-Zadeh, A., Matenco, L., Radulian, M., Cloetingh, S., Panza, G., 2012. Geodynamic and intermediate-depth seismicity in Vrancea (the south-eastern Carpathians): current state-of-the-art. Tectonophysics 530–531, 50–79.

Juvigné, E., 1992. Distribution of widespread Late Glacial and Holocene tephra beds in the French Central Massif. Quat. Int. 13 (14), 180–185.

Juvigné, E., Kroonenberg, S.B., Weldkamp, A., El Arabi, A., Vernet, G., 1992. Widespread Allerød and Boreal trachyandesitic to trachytic tephra layers as stratigraphical markers in the Massif Central, France. Quaternaire 3, 137–146.

Juvigné, E., Gewelt, M., Gilot, E., Hurtgen, C., Seghedi, I., Szakács, A., Gábris, Gy, Hadnagy, Á., Horváth, E., 1994. Une éruption vieille d'environ 10,700 ans (14C) dans les Carpates orientales (Roumanie). C. R. Acad. Sci. Ser. II Paris 318, 1233–1238.

Karátson, D., 2007. A Börzsönytől a Hargitáig — vulkanológia, felszínfejlődés, ősföldrajz. Typotex Kiadó, Budapest ((From Börzsöny to Harghita Mts. — volcanology, surface evolution, paleogeography; in Hungarian) 463 pp.).

Karátson, D., Timár, G., 2005. Comparative volumetric calculations of two segments of the Neogene/Quaternary volcanic chain using SRTM elevation data: implications for erosion and magma output rates. Z. Geomorphol. Suppl. 140, 19–35.

Karátson, D., Telbisz, T., Harangi, S., Magyari, E., Dunkl, I., Kiss, B., Jánosi, C., Veres, D., Braun, M., Fodor, E., Biró, T., Kósik, S., von Eynatten, H., Lin, D., 2013. Morphometrical and geochronological constraints on the youngest eruptive activity in East-Central Europe at the Ciomadul (Csomád) lava dome complex, East Carpathians. J. Volcanol. Geotherm. Res. 255, 43–56.

Kiss, B., Harangi, S., Ntaflos, T., Mason, P.R.D., Pál-Molnár, E., 2014. Amphibole perspective to unravel pre-eruptive processes and conditions in volcanic plumbing systems beneath intermediate arc volcanoes: a case study from Ciomadul volcano (SE Carpathians). Contrib. Mineral. Petrol. 167, 986.

Klemetti, E.W., Clynne, M.A., 2014. Localized rejuvenation of a crystal mush recorded in zircon temporal and compositional variation at the Lassen Volcanic Center, Northern California. PLoS ONE 9, e113157.

Lane, C.S., Andric, M., Cullen, V.L., Blockley, S.P.E., 2011. The occurrence of distal Icelandic and Italian tephra in the Lateglacial of Lake Bled, Slovenia. Quat. Sci. Rev. 30, 1013–1018.

Lane, C.S., Blockley, S.P.E., Lotter, A.F., Finsinger, W., Filippi, M.L., Matthews, I.P., 2012. A regional tephrostratigraphic framework for central and southern European climate archives during the Last Glacial to Interglacial transition: comparisons north and south of the Alps. Quat. Sci. Rev. 36, 50–58.

Lexa, J., Seghedi, I., Németh, K., Szakács, A., Konečny, V., Pécskay, Z., Fülöp, A., Kovacs, M., 2010. Neogene–Quaternary volcanic forms in the Carpathian–Pannonian Region: a review. Cen. Eur. J. Geosci. 2, 207–270.

Martí, J., Planaguma, L., Geyer, A., Canal, E., Pedrazzi, D., 2011. Complex interaction between Strombolian and phreatomagmatic eruptions in the Quaternary monogenetic volcanism of the Catalan Volcanic Zone (NE of Spain). J. Volcanol. Geotherm. Res. 201, 178–193.

Martin, M., Wenzel, F., CALIXTO Working Group, 2006. High-resolution teleseismic body wave tomography beneath SE Romania: II. Imaging of a slab detachment scenario. Geophys. J. Int. 164, 579–595.

Mason, P.R.D., Downes, H., Seghedi, I., Szakács, A., Thirlwall, M.F., 1995. Low-pressure evolution of magmas from the Calimani, Gurghiu and Harghita Mountains, East Carpathians. Acta Vulcanol. 7, 43–52.

Mason, P.R.D., Downes, H., Thirlwall, M., Seghedi, I., Szakács, A., Lowry, D., Mattey, D., 1996. Crustal assimilation as a major petrogenetic process in the East Carpathian Neogene and Quaternary continental margin arc, Romania. J. Petrol. 37, 927–959.

Miller, J.S., Matzel, J.E.P., Miller, C.F., Burgess, S.D., Miller, R.B., 2007. Zircon growth and recycling during the assembly of large, composite arc plutons. J. Volcanol. Geotherm. Res. 167, 282–299.

Moriya, I., Okuno, M., Nakamura, E., Szakács, A., Seghedi, I., 1995. Last eruption and its 14C age of Ciomadul volcano, Romania. Summaries of Researches using AMS at Nagoya University 6 pp. 82–91.

Moriya, I., Okuno, M., Nakamura, T., Ono, K., Szakács, A., Seghedi, I., 1996. Radiocarbon ages of charcoal fragments from the pumice flow deposits of the last eruption of Ciomadul volcano, Romania. Summaries of Research using AMS at Nagoya University VII pp. 255–257.

Morley, M.W., Woodward, J.C., 2011. The Campanian Ignimbrite (Y5) tephra at Crvena Stijena Rockshelter, Montenegro. Quat. Res. 75, 683–696.

Nowell, D.A.G., Jones, M.C., Pyle, D.M., 2006. Episodic Quaternary volcanism in France and Germany. J. Quat. Sci. 21, 645–675.

Oncescu, M.C., Burlacu, V., Anghel, M., Smalberger, V., 1984. Three-dimensional p-wave velocity image under the Carpathian arc. Tectonophysics 106, 305–319.

Pécskay, Z., Szakács, A., Seghedi, I., Karátson, D., 1992. Contributions to the geochronology of Mt. Cucu volcano and the South Harghita (East Carpathians, Romania). Földt. Közl. (Bull. Hung. Geol. Soc.) 122, 265–286.

Pécskay, Z., Edelstein, O., Seghedi, I., Szakacs, A., Kovacs, M., Crihan, M., Bernad, A., 1995. K_Ar datings of Neogene–Quaternary calc-alkaline volcanic rocks in Romania. Acta Vulcanol. 7, 53–61.

Peltz, S., Vajdea, E., Balogh, K., Pécskay, Z., 1987. Contribution to the geochronological study of the volcanic processes in the Calimani and Harghita Mts. Dari S. Sed. Inst. Geol. Geofiz. 72–73, 323–338.

Popa, M., Radulian, M., Szakács, A., Seghedi, I., Zaharia, B., 2012. New seismic and tomography data in the southern part of the Harghita mountains (Romania, Southeastern Carpathians): connection with recent volcanic activity. Pure Appl. Geophys. 169, 1557–1573.

Prescott, J.R., Hutton, J.T., 1994. Cosmic ray contribution to dose rates for luminescence and ESR dating: large depth and long-term time variations. Radiat. Meas. 23, 497–500.

Press, W.H., Teukolsky, S.A., Vetterling, W.T., Flannery, B.P., 2002. Numerical Recipes in C++: The Art of Scientific Computing. Cambridge University, New York (688 pp.).

Puiguriguer, M., Alcalde, G., Bassols, E., Burjachs, F., Expósito, I., Planagumà, L., Saña, M., Yll, E., 2012. ^{14}C dating of the last Croscat volcano eruption (Garrotxa Region, NE Iberian Peninsula). Geol. Acta 10, 43–47.

Pyle, D.M., Ricketts, G.D., Margari, V., van Andel, T.H., Sinitsyn, A.A., Praslov, N.D., Lisitsyn, S., 2006. Wide dispersal and deposition of distal tephra during the Pleistocene 'Campanian Ignimbrite/Y5' eruption, Italy. Quat. Sci. Rev. 25, 2713–2728.

Rees-Jones, J., 1995. Optical dating of young sediments using fine-grain quartz. Ancient TL 13, 9–14.

Reid, M.R., Coath, C.D., Harrison, T.M., McKeegan, K.D., 1997. Prolonged residence times for the youngest rhyolites associated with Long Valley Caldera: ^{230}Th–^{238}U ion microprobe dating of young zircons. Earth Planet. Sci. Lett. 150, 27–39.

Reiners, P.W., 2005. Zircon (U–Th)/He thermochronometry. Rev. Mineral. Geochem. 58, 151–179.

Santacroce, R., Cioni, R., Marianelli, P., Sbrana, A., Sulpizio, R., Zanchetta, G., Donahue, D.J., Joron, J.L., 2008. Age and whole rock-glass compositions of proximal pyroclastics from the major explosive eruptions of Somma–Vesuvius: a review as a tool for distal tephrostratigraphy. J. Volcanol. Geotherm. Res. 177, 1–18.

Sañudo-Wilhelmy, S.A., Flegal, A.R., 1994. Temporal variations in lead concentrations and isotopic composition in the Southern California Bight. Geochim. Cosmochim. Acta 58, 3315–3320.

Schmidt, R., van den Bogaard, C., Merkt, J., Muller, J., 2002. A new Lateglacial chronostratigraphic tephra marker for the south-eastern Alps: the Neapolitan Yellow Tuff (NYT) in Langsee (Austria) in the context of a regional biostratigraphy and palaeoclimate. Quat. Int. 88, 45–56.

Schmincke, H.-U., 2007. The Quaternary volcanic fields of the East and West Eifel (Germany). In: Ritter, R., Christensen, U. (Eds.), Mantle Plumes — A Multidisciplinary Approach. Springer, pp. 241–322.

Schmitt, A.K., 2006. Laacher See revisited: high spatial resolution zircon dating indicates rapid formation of a zoned magma chamber. Geology 34, 597–600.
Schmitt, A.K., Stockli, D.F., Hausback, B.P., 2006. Eruption and magma crystallization ages of Las Tres Vírgenes (Baja California) constrained by combined $^{230}Th/^{238}U$ and (U–Th)/He dating of zircon. J. Volcanol. Geotherm. Res. 158, 281–295.
Schmitt, A.K., Stockli, D.F., Niedermann, S., Lovera, O.M., Hausback, B.P., 2010a. Eruption ages of Las Tres Vírgenes volcano (Baja California): a tale of two helium isotopes. Quat. Geochronol. 5, 503–511.
Schmitt, A.K., Stockli, D.F., Lindsay, J.M., Robertson, R., Lovera, O.M., Kislitsyn, R., 2010b. Episodic growth and homogenization of plutonic roots in arc volcanoes from combined U–Th and (U–Th)/He zircon dating. Earth Planet. Sci. Lett. 295, 91–103.
Schmitt, A.K., Danišík, M., Evans, N., Siebel, W., Kiemele, E., Aydin, F., Harvey, J.C., 2011. Acigöl rhyolite field, Central Anatolia (part 1): high-resolution dating of eruption episodes and zircon growth rates. Contrib. Mineral. Petrol. 162, 1233–1247.
Schmitt, A.K., Danišík, M., Siebel, W., Elitok, Ö., Chang, Y.-W., Shen, C.C., 2014. Late Pleistocene zircon ages for intracaldera domes at Gölcük (Isparta, Turkey). J. Volcanol. Geotherm. Res. 286, 24–29.
Seghedi, I., Downes, H., 2011. Geochemistry and tectonic development of Cenozoic magmatism in the Carpathian–Pannonian region. Gondwana Res. 20, 655–672.
Seghedi, I., Szakács, A., Udrescu, C., Stoian, M., Grabari, G., 1987. Trace element geochemistry of the South Harghita volcanics (East Carpathians): calc-alkaline and shoshonitic association. Dari S. Sed. Inst. Geol. Geofiz. 72–73, 381–397.
Seghedi, I., Downes, H., Szakacs, A., Mason, P.R.D., Thirlwall, M.F., Rosu, E., Pecskay, Z., Marton, E., Panaiotu, C., 2004. Neogene–Quaternary magmatism and geodynamics in the Carpathian–Pannonian region: a synthesis. Lithos 72, 117–146.
Seghedi, I., Downes, H., Harangi, S., Mason, P.R.D., Pécskay, Z., 2005. Geochemical response of magmas to Neogene–Quaternary continental collision in the Carpathian–Pannonian region: a review. Tectonophysics 410 (1–4), 485–499.
Sperner, B., Lorenz, F., Bonjer, K., Hettel, S., Muller, B., Wenzel, F., 2001. Slab break-off — abrupt cut or gradual detachment? New insights from the Vrancea Region (SE Carpathians, Romania). Terra Nova 13, 172–179.
Stelten, M.E., Cooper, K.M., 2012. Constraints on the nature of the subvolcanic reservoir at South Sister volcano, Oregon from U-series dating combined with sub-crystal trace-element analysis of plagioclase and zircon. Earth Planet. Sci. Lett. 313–314, 1–11.
Szabó, C., Harangi, S., Csontos, L., 1992. Review of Neogene and Quaternary volcanism of the Carpathian–Pannonian region. Tectonophysics 208, 243–256.
Szakács, A., Seghedi, I., 1986. Chemical diagnosis of the volcanics from the most southernmost part of the Harghita mountains—proposal for a new nomenclature. Rev. Roum. Géol. Géophys. Géogr. Géol. 30, 41–48.
Szakács, A., Seghedi, I., 1989. Base surge deposits in the Ciomadul Massif (South Harghita Mts.). Dari S. Sed. Inst. Geol. Geofiz. 74/1, 175–180.
Szakács, A., Seghedi, I., 1995. The Călimani–Gurghiu–Harghita volcanic chain, East Carpathians, Romania: volcanological features. Acta Volcanol. 7, 145–155.
Szakács, A., Seghedi, I., 2013. The relevance of volcanic hazard in Romania: is there any? Environ. Eng. Manag. J. 12, 125–135.
Szakács, A., Seghedi, I., Pécskay, Z., 1993. Peculiarities of South Harghita Mts. as terminal segment of the Carpathian Neogene to Quaternary volcanic chain. Rev. Roum. Géol. Géophys. Géogr. Géol. 37, 21–37.
Szakács, A., Seghedi, I., Pécskay, Z., Mirea, V., 2015. Eruptive history of a low frequency and low-output rate Pleistocene volcano, Ciomadul, South Harghita Mts., Romania. Bull. Volcanol. 77, 12. http://dx.doi.org/10.1007/s00445-014-0894-7.
Tanţău, I., Reille, M., De Beaulieu, J.L., Fărcas, S., Goslar, T., Paterne, M., 2003. Vegetation history in the eastern Romanian Carpathians: pollen analysis of two sequences from the Mohoş crater. Veg. Hist. Archaeobotany 12, 113–125.
Thiel, C., Buylaert, J.-P., Murray, A., Terhorst, B., Hofer, I., Tsukamoto, S., Frechen, M., 2011. Luminescence dating of the Stratzing loess profile (Austria) — testing the potential of an elevated temperature post-IR IRSL protocol. Quat. Int. 234, 23–31.
Thomsen, K.J., Jain, M., Murray, A.S., Denby, P.M., Roy, N., Bøtter-Jensen, L., 2008. Minimizing feldspar OSL contamination in quartz UV-OSL using pulsed blue stimulation. Radiat. Meas. 43, 752–757.
van den Bogaard, P., 1995. $^{40}Ar/^{39}Ar$ ages of sanidine phenocrysts from Laacher See Tephra (12,900 BP): chronostratigraphic and petrological significance. Earth Planet. Sci. Lett. 133, 163–174.
Vaselli, O., Minissale, A., Tassi, F., Magro, G., Seghedi, I., Ioane, D., Szakács, A., 2002. A geochemical traverse across the Eastern Carpathians (Romania): constraints on the origin and evolution of the mineral water and gas discharges. Chem. Geol. 182, 637–654.
Veres, D., Lane, S.C., Timar-Gabor, A., Hambach, H., Constantin, D., Szakács, A., Fülling, A., Onac, B.P., 2013. The Campanian Ignimbrite/Y5 tephra layer — a regional stratigraphic marker for isotope stage 3 deposits in the Lower Danube region, Romania. Quat. Int. 293, 22–33.
Vernet, G., Raynal, J.P., 2008. La Formation de Marsat et le Téphra CF7, marqueurs distaux d'éruptions trachytiques violentes de la chaîne des Puys au Boréal. Quaternaire 19, 97–106.
Vinkler, A.P., Harangi, S., Ntaflos, T., Szakács, A., 2007. A Csomád vulkán (Keleti-Kárpátok) horzsaköveinek kőzettani és geokémiai vizsgálata — petrogenetikai következtetések (Petrology and geochemistry of pumices from the Ciomadul volcano (Eastern Carpathians) — implications for petrogenetic processes). Földt. Közl. (Bull. Hung. Geol. Soc.) 137, 103–128.
Vogel, H., Zanchetta, G., Sulpizio, R., Wagner, B., Nowaczyk, N., 2010. A tephrostratigraphic record for the last glacial–interglacial cycle from Lake Ohrid, Albania and Macedonia. J. Quat. Sci. 25, 320–338.
Wendt, I., Carl, C., 1985. U/Pb dating of discordant 0.1 Ma old secondary U minerals. Earth Planet. Sci. Lett. 73, 278–284.
Wenzel, F., Lorenz, F., Sperner, B., Oncescu, M.C., 1999. Seismotectonics of the Romanian Vrancea area. In: Wenzel, F., Lungu, D., Novak, O. (Eds.), Vrancea Earthquakes: Tectonics, Hazard and Risk Mitigation. Kluwer Academic Publishers, Dordrecht, pp. 15–26.
Wiedenbeck, M., Allé, P., Corfu, F., Griffin, W.L., Meier, M., Oberli, F., von Quadt, A., Roddick, J.C., Spiegel, W., 1995. Three natural zircon standards for U–Th–Pb, Lu–Hf, trace element and REE analyses. Geostand. Newslett. 19, 1–23.